Published in final edited form as:
Nature. 2021 January 01; 589(7842): 442–447. doi:10.1038/s41586-020-03071-0.

RANK links thymic regulatory T cells to fetal loss and gestational diabetes in pregnancy

Magdalena Paolino[1,2,3,†], **Rubina Koglgruber**[1], **Shane J. F. Cronin**[1], **Iris Uribesalgo**[1], **Esther Rauscher**[1], **Jürgen Harreiter**[4], **Michael Schuster**[5], **Dagmar Bancher-Todesca**[6], **Blanka Pranjic**[1], **Maria Novatchkova**[1], **Juan P. Fededa**[1,7], **Andrea J. White**[8], **Verena Sigl**[1], **Sabine Dekan**[9], **Thomas Penz**[5], **Christoph Bock**[5,10], **Lukas Kenner**[9,11,12,13,14], **Georg A. Holländer**[15,16,17], **Graham Anderson**[8], **Alexandra Kautzky-Willer**[4,18], **Josef M. Penninger**[1,19,†]

[1]Institute of Molecular Biotechnology of the Austrian Academy of Sciences (IMBA), Vienna, Austria [2]Department of Medicine Solna, Karolinska Institutet, Stockholm, Sweden [3]Karolinska University Hospital, Stockholm, Sweden [4]Gender Medicine Unit, Division of Endocrinology and Metabolism, Department of Medicine III, Medical University of Vienna, Vienna, Austria [5]Research Center for Molecular Medicine of the Austrian Academy of Science (CeMM), Vienna, Austria [6]Division of Obstetrics and Feto-Maternal Medicine, Department of Obstetrics and Gynecology, Medical University of Vienna, Vienna, Austria [7]Instituto de Investigaciones Biotecnológicas “Dr. Rodolfo A. Ugalde”, IIB-UNSAM, IIBIO-CONICET, Universidad Nacional de San Martín, Buenos Aires, Argentina [8]Institute for Immunology and Immunotherapy, Institute for Biomedical Research, Medical School, University of Birmingham, Birmingham, UK [9]Department of Pathology, Medical University of Vienna, Vienna, Austria [10]Department of Laboratory Medicine, Medical University of Vienna, Vienna, Austria [11]Division of Experimental and Translational Pathology, Department of Pathology, Medical University Vienna, Vienna, Austria [12]Center for Biomarker Research in Medicine (CBmed), Graz, Austria [13]Unit for Laboratory Animal Pathology, University of Veterinary Medicine Vienna, Vienna, Austria [14]Christian Doppler Laboratory for Applied Metabolomics (CDL-AM), Medical University of Vienna, Vienna, Austria [15]Paediatric Immunology, Department of Biomedicine, University of Basel and University Children’s Hospital Basel, Basel, Switzerland [16]Department of Paediatrics and The Weatherall Institute of Molecular Medicine, University of Oxford, Oxford, UK [17]Department of Biosystems Science and Engineering, ETH Zurich, Basel, Switzerland [18]Austrian Institute for Gender Medicine, Gars am Kamp, Austria [19]Department of

[†]**Correspondence and requests for materials** should be addressed to M.P. or J.M.P. magdalena.paolino@ki.se; josef.penninger@imba.oeaw.ac.at.

Author contributions.

All experiments were performed by M.P. with the help of: R.K. in the maintenance of mouse colony and metabolic studies and E.R. for breeding and timed pregnancies; I.U. in qPCR analysis; S.J.F.C. in adoptive transfer experiments and T_{reg} cell suppression assays; B.P. in mouse dissections and J.P.F. in confocal imaging. V.S. helped with sex-hormone in vivo experiments. A.J.W. performed FTOC cultures. L.K. and S.D. performed the pathology analysis of placentas and pancreas. J.H., D.B.-T. and A.K.-W. collected human samples and anthropometric data on pregnant women. T.P. and C.B. performed Smart-seq2 sequencing on T_{reg} cells and M.S. performed bioinformatics analyses on the Smart-seq2 data. M.N. performed bioinformatics analyses on the QuantSeq data and GSEA analyses. G.A.H. provided the *Foxn1* ^{cre} expressing mice. G.A. provided expertise in experimental design, training and data analysis of FTOCs and confocal microscopy, as well as key reagents. M.P. together with J.M.P. designed the experiments and wrote the manuscript.

Competing interests The authors declare no competing interests.

Europe PMC Funders Author Manuscripts

Medical Genetics, Life Sciences Institute, University of British Columbia, Vancouver, British Columbia, Canada

Abstract

Successful pregnancies rely on adaptations within the mother[1], including marked changes within the immune system[2]. It has long been known that the thymus, the central lymphoid organ, changes markedly during pregnancy[3]. However, the molecular basis and importance of this process remain largely obscure. Here we show that the osteoclast differentiation receptor RANK[4,5] couples female sex hormones to rewiring of the thymus during pregnancy. Genetic deletion of *Rank* (also known as *Tnfrsf11a*) in thymic epithelial cells results in impaired thymic involution and blunted expansion of natural regulatory T (T_{reg}) cells in pregnant female mice. Sex hormones, in particular progesterone, drive the development of thymic T_{reg} cells through RANK in a manner that depends on $AIRE^+$ medullary thymic epithelial cells and depletion of *Rank* in the thymic epithelium results in reduced accumulation of natural T_{reg} cells in the placenta, accompanied by an increased number of miscarriages. Thymic deletion of *Rank* also resulted in impaired accumulation of T_{reg} cells in visceral adipose tissue, associated with enlarged adipocyte size, tissue inflammation, enhanced maternal glucose intolerance, fetal macrosomia, and a long-lasting transgenerational alteration in glucose homeostasis; key hallmarks of gestational diabetes. Transplantation of T_{reg} cells rescued fetal loss, maternal glucose intolerance and fetal macrosomia. In human pregnancies, gestational diabetes also correlates with a reduced number of T_{reg} cells in the placenta. Our findings show that RANK promotes the hormone-mediated development of thymic T_{reg} cells during pregnancy and expand the functional role of maternal T_{reg} cells to gestational diabetes and the transgenerational metabolic rewiring of glucose homeostasis.

During pregnancy, sex hormones help to coordinate marked anatomical and physiological adaptations in the pregnant mother in order to safeguard fetal development[1]. The receptor activator of NF-κB ligand (RANK), its ligand RANKL and the decoy osteoprotegerin regulate—under the control of female sex hormones—bone remodelling and the development of lactating mammary glands during pregnancy[6,7]. In the thymus, RANK signalling regulates the maturation of AIRE- and CD80-expressing medullary thymic epithelial cells (mTECs)[8], which have been implicated in the development of natural thymic T_{reg} cells[9]. We therefore hypothesized that RANK could mediate vital thymic adaptations during pregnancy.

In the thymi of pregnant wild-type mice, *Rank* and *Aire* mRNA levels were upregulated during pregnancy, and pregnant female mice displayed increased numbers of $AIRE^+$mTECs (Extended Data Fig. 1a–c). We next deleted *Rank* in thymic epithelial cells by crossing *Rank* $^{floxed/floxed}$ with *Foxn1* $^{cre/wt}$ mice to generate *Rank* $^{floxed/floxed}$ *Foxn1* $^{wt/wt}$ (hereafter, *Rank* ^{WT}) and *Rank* $^{floxed/floxed}$ *Foxn1* $^{Cre/wt}$ animals (hereafter, *Rank* $^{\Delta Foxn1}$). We observed efficient deletion in the thymic medulla and reduced numbers of $AIRE^+$mTECs in *Rank* $^{\Delta Foxn1}$ mice (Fig. 1a and Extended Data Fig. 1d). The findings in *Rank* $^{\Delta Foxn1}$ mice were corroborated by conditional *Rank* deletion in mTECs using *K5* ^{cre} (*K5* is also known as *Krt5*) mice (*Rank* $^{\Delta K5}$) (Extended Data Fig. 1e–g). *Rank* $^{\Delta Foxn1}$ and *Rank* $^{\Delta K5}$ females

appeared overtly normal, exhibiting normal thymic size, thymic organization, thymocyte subsets, normal splenic T cell populations, percentages of thymic and splenic T_{reg} cells, and suppressive activities of splenic T_{reg} cells (Extended Data Fig. 1h–r). Thus, in non-pregnant female mice, the genetic inactivation of *Rank* in the thymic epithelium markedly reduces the numbers of mature mTECs, without any apparent effect on the thymic architecture, and the development of thymocytes or T_{reg} cells.

During pregnancy, the thymus undergoes marked changes, including partial involution, increased medullary-to-cortex ratios and altered thymocyte development; all of these thymic adaptions were altered in $Rank^{\Delta Foxn1}$ mice with syngeneic pregnancies (Extended Data Fig. 2a–g). Increased numbers of $AIRE^{+}$mTECs and progressive thymic T_{reg} cell expansion in pregnant female mice depended on *Rank* expression in the thymic epithelium (Fig. 1b–d and Extended Data Fig. 2h, i). Impaired thymic T_{reg} cell expansion was confirmed in pregnant $Rank^{\Delta K5}$ female mice (Extended Data Fig. 2j). Whereas increased CTLA-4, neuropilin-1 and Helios expression as well as increased proliferation and improved survival of thymic T_{reg} cells occurred in both pregnant $Rank^{WT}$ and $Rank^{\Delta Foxn1}$ female mice, $Rank^{\Delta Foxn1}$ mice exhibited impaired differentiation of $CD69^{+}CCR9^{+}CCR7^{-}$ to mature $CD69^{-}CCR9^{-}CCR7^{+}CD4^{+}CD25^{+}FOXP3^{+}T_{reg}$ cells in pregnancy (Extended Data Fig. 2k–n). Expansion of $AIRE^{+}$mTECs and thymic T_{reg} cells was confirmed in allogeneic pregnancies and was dependent on RANK expression in mTECs (Extended Data Fig. 3a–d). RNA-sequencing analysis showed that pregnancy is associated with marked changes in the molecular profiles of thymic T_{reg} cells; *Rank* deletion in mTECs changed the transcriptome and T-cell-receptor (TCR) repertoire of T_{reg} cells in pregnant as well as non-pregnant female mice (Extended Data Fig. 3e–g and Supplementary Table 1). Finally, RANK stimulation in fetal thymic organ cultures resulted in a marked increase in $FOXP3^{+}T_{reg}$ cells, which could be reverted by the decoy osteoprotegerin (Extended Data Fig. 4a, b). Thus, loss of RANK expression in mTECs impairs thymic T_{reg} cell expansion during pregnancy.

Female mice displayed thymic involution as well as an upregulation in the levels of *Rank* and *Aire* mRNA in the thymus in response to synthetic progestin, and to a lesser extent in response to oestrogen, regardless of whether the mice were ovariectomized (Fig. 1e and Extended Data Fig. 4c, d). Progestin increased $AIRE^{+}$ mTEC and $FOXP3^{+}$Thymic T_{reg} cell numbers in ovariectomized $Rank^{WT}$ female mice, but not in ovariectomized $Rank^{\Delta Foxn1}$ littermates (Fig. 1f, g) nor in ovariectomized $Rank^{\Delta K5}$ female mice (Extended Data Fig. 4e, f). Progestin-expanded $CD4^{+}FOXP3^{+}T_{reg}$ cells expressed high levels of the thymic T_{reg} cell marker neuropilin-1[10] (Extended Data Fig. 4g). *Rank*-dependent expansion of T_{reg} cells was also induced by treatment with natural progesterone (Extended Data Fig. 4h, i). Thymic expression of the progesterone receptor was comparable among ovariectomized, non-pregnant and pregnant $Rank^{WT}$ and $Rank^{\Delta Foxn1}$ female mice (Extended Data Fig. 4j). Thus, progesterone induces thymic T_{reg} cell development by acting on $RANK^{+}$mTECs.

Next, we investigated the consequences of RANK-regulated thymic T_{reg} cell expansion during pregnancy. We observed similar numbers and suppressive activities of T_{reg} cells as well as $CD4^{+}$ and $CD8^{+}$T cells in the spleens of non-pregnant and mid-to-late stage pregnant $Rank^{WT}$ and $Rank^{\Delta Foxn1}$ female mice, and there were no overt signs of autoimmunity in pregnant $Rank^{\Delta Foxn1}$ female mice (Extended Data Fig. 4k–u and Supplementary Table 1).

Whereas healthy pregnancies, in both humans and mice, correlate with the accumulation of T_{reg} cells in the placenta[11,12], placentas from *Rank* $^{\Delta Foxn1}$ dams displayed significantly lower numbers of T_{reg} cells, in particular those of thymic origin, which were defined[10,13] as neuropilin-1^{high}Helios^{high} (Fig. 1h and Extended Data Fig. 5a–c). We observed reduced proliferation as well as differential expression and a less-restricted TCR repertoire in placental T_{reg} cells of *Rank* $^{\Delta Foxn1}$ mice, whereas they were similar among CD4^{+}FOXP3^{-} placental conventional T cells of both genotypes (Extended Data Fig. 5d–h and Supplementary Table 1). RNA-sequencing analysis revealed that placental T_{reg} cells from *Rank* $^{\Delta Foxn1}$ dams displayed differential gene expression compared with *Rank* ^{WT} controls, with allograft rejection and inflammatory responses as the top overexpressed gene sets (Extended Data Fig. 5i, j and Supplementary Table 2). In line with the reduced numbers and molecular alterations in placental T_{reg} cells, fetal resorptions rates were three times higher in pregnant *Rank* $^{\Delta Foxn1}$ and *Rank* $^{\Delta K5}$ mice compared with pregnant *Rank* ^{WT} controls (Fig. 1i–l). The total numbers of fetuses per mother as well as the male-to-female sex ratios were comparable (Extended Data Fig. 5k, l). Thus, the deletion of RANK in the thymic epithelium results in perturbed natural T_{reg} cells in the placenta and increased fetal loss.

Surprisingly, viable fetuses of *Rank* $^{\Delta Foxn1}$ dams were significantly heavier at term regardless of sex, *Rank* heterozygosity or litter sizes (Fig. 2a–c and Extended Data Fig. 5m), a hallmark of gestational diabetes in humans[14]. Pregnant *Rank* $^{\Delta Foxn1}$ female mice displayed higher glucose levels in the placenta, and hyperglycaemia and hyperinsulinaemia in the serum (Fig. 2d–f); non-pregnant cohorts were indistinguishable (Extended Data Fig. 5n, o). Similarly to humans[15], late pregnancy in mice was associated with decreased glucose tolerance; *Rank* $^{\Delta Foxn1}$ dams also showed significantly higher glucose response curves (Fig. 2g, h), which is indicative of glucose intolerance. There was no apparent difference in pregnancy-associated β-islet expansion[16] and glucose levels were normalized in pregnant *Rank* $^{\Delta Foxn1}$ mice after fasting (Extended Data Fig. 5p–t), arguing against defects in insulin production and/or secretion. Previous studies in male mice have shown that T_{reg} cells can alter glucose homeostasis by regulating inflammation in the visceral white adipose tissue (VAT)[17–19]. During pregnancy, we observed an accumulation of thymic T_{reg} cells in the VAT of *Rank* ^{WT}, but not *Rank* $^{\Delta Foxn1}$, dams (Fig. 2i and Extended Data Fig. 6a, b). We also found molecular differences between VAT T_{reg} cells from *Rank* ^{WT} and *Rank* $^{\Delta Foxn1}$ dams, including TCR expression, inflammation, metabolism, chemokine and cytokine signalling (Extended Data Fig. 6c–i and Supplementary Tables 1, 3). Concomitantly, the VAT of *Rank* $^{\Delta Foxn1}$ dams had a reduced glucose uptake capacity (Fig. 2j). T_{reg} cell numbers in aortic lymph nodes, lungs, kidneys, exocrine pancreas and β-islets remained unchanged (Extended Data Fig. 6j–l). Body weight changes, thymic and VAT T_{reg} cell numbers, glucose tolerance and insulin levels were comparable between non-pregnant *Rank* ^{WT} and *Rank* $^{\Delta Foxn1}$ female mice that were fed a high-fat diet (HFD) (Extended Data Fig. 6m–r). Thus, inactivation of *Rank* in the thymic epithelium results in impaired accumulation of T_{reg} cells and reduced glucose uptake in the VAT of pregnant female mice, and is associated with increased gestational glucose intolerance and larger pups.

To demonstrate a causal role of thymic T_{reg} cells in maternal metabolism and fetal loss, we established an adoptive T_{reg} cell transfer model, showing that FOXP3–GFP^{+}neuropilin-1^{high} T_{reg} cells from pregnant wild-type donors selectively home to the placenta; reconstitution of

Rank $^{\Delta Foxn1}$ dams with regulatory T cells from pregnant *Rank* ^{WT} females restored the impaired placental T_{reg} cell numbers and prevented miscarriages found in *Rank* $^{\Delta Foxn1}$ dams (Fig. 3a–d and Extended Data Fig. 7a–l). The transplantation of pregnancy-associated T_{reg} cells also resulted in the homing of T_{reg} cells to the VAT and restoration of the number of T_{reg} cells, glucose tolerance, glucose uptake and expression of the glucose transporter *Glut4* (also known as *Slc2a4*) in the VAT of *Rank* $^{\Delta Foxn1}$ pregnant mice (Fig. 3e–g and Extended Data Fig. 7a–d). In contrast to the placenta, transfer of T_{reg} cells from non-pregnant *Rank* ^{WT} *Foxp3* $^{GFP/GFP}$ and from pregnant *Rank* $^{\Delta Foxn1}$ *Foxp3* $^{GFP/GFP}$ female mice could improve glucose tolerance and VAT T_{reg} cell numbers in recipient *Rank* $^{\Delta Foxn1}$ dams (Extended Data Fig. 7m–o). RNA-sequencing analysis revealed significant differences in gene expression between the VAT of *Rank* $^{\Delta Foxn1}$and *Rank* ^{WT} dams, including TNF-dependent inflammation and oxidative phosphorylation (Fig. 3h and Extended Data Fig. 8a–e) —gene signature pathways linked to insulin resistance[20,21]. T_{reg} cell transplantation restored gene expression in the VAT of *Rank* $^{\Delta Foxn1}$ dams (Fig. 3h, i and Extended Data Fig. 8a–e). The VAT of *Rank* $^{\Delta Foxn1}$ dams was significantly larger, showing enlarged adipocytes and marked macrophage infiltration; all of which was restored by T_{reg} cell transplantation (Extended Data Fig. 8f–k). Finally, reconstitution of T_{reg} cell numbers during pregnancy prevented macrosomia in the offspring of *Rank* $^{\Delta Foxn1}$ dams (Fig. 3j). Thus, reconstitution of *Rank* $^{\Delta Foxn1}$ dams with regulatory T cells from pregnant *Rank* ^{WT} female mice prevented miscarriages, VAT inflammation, gestational glucose intolerance and fetal macrosomia.

In humans, children born to women with gestational diabetes can have long-term health complications, such as proclivity to glucose intolerance and obesity[22,23]. We therefore followed the fate of macrosomic pups born to *Rank* $^{\Delta Foxn1}$ mothers, observing increased body weights throughout the entire timespan of follow-up, a phenotype observed in both male and female mice regardless of whether the mice were fed normal chow, HFD or nurtured by wild-type mothers (Fig. 4a, b and Extended Data Fig. 9a–d). We consistently observed hyperinsulinaemia in male and female offspring of *Rank* $^{\Delta Foxn1}$ mothers, again under both diet regiments; this effect was normalized after fasting (Fig. 4c and Extended Data Fig. 9e–g). When fed normal chow, female, but not male, offspring of *Rank* $^{\Delta Foxn1}$ mothers had higher glucose levels and impaired glucose tolerance (Extended Data Fig. 9h–k). When fed a HFD, both male and female offspring of *Rank* $^{\Delta Foxn1}$ mothers exhibited hyperglycaemia and marked glucose intolerance (Fig. 4d, e and Extended Data Fig. 9l, m). Similar to patients with type 1 and type 2 diabetes[24,25], offspring of *Rank* $^{\Delta Foxn1}$ mothers have a reduced β-islet mass (Fig. 4f). Male offspring from *Rank* $^{\Delta Foxn1}$ mothers had reduced T_{reg} cell frequencies when fed a HFD and, when fed normal chow, showed an increase in the size of adipocytes as well as altered frequencies of T_{reg} cells and macrophages in the VAT (Extended Data Fig. 9n–q). Thus, ablation of *Rank* in the thymic epithelium results in glucose intolerance in pregnant female mice and transgenerationally in their offspring, with long-lasting effects.

The estimated rates of gestational diabetes have reached up to 18–39% of human pregnancies[26,27]. We therefore assessed whether regulatory T cells are also altered in a clinical cohort study of women with gestational diabetes compared with women matched for body-mass index who had a normal glucose tolerance, and additionally matched for the sex of the babies, and week and mode of delivery (Fig. 4g and Extended Data Fig. 10a–f). As

expected, babies born to mothers with gestational diabetes exhibited an increased birth weight and enhanced C-peptide levels, as a marker for insulin levels, in the cord blood (Fig. 4h and Extended Data Fig. 10g). Notably, we observed reduced T_{reg} cell numbers in the placentas of women with gestational diabetes, regardless of diet or insulin treatments (Fig. 4i–k and Extended Data Fig. 10h, i). Therefore, in line with our studies in pregnant *Rank* $^{\Delta Foxn1}$ mice, reduced T_{reg} cell numbers in the placenta correlate with gestational diabetes in human pregnancy.

How the immune system deals with the fetus during pregnancy remains unclear and is a central question of immunology and evolution. Various layers of immune regulation at the maternal–fetal interface have been linked to viable pregnancies[2], including the presence of T_{reg} cells[11,12]. Despite having a comparable suppression potency[28,29], only pregnancy-associated T_{reg} cells, but not T_{reg} cells from non-pregnant female mice, can rescue miscarriages[29], suggesting a dedicated development and/or function for pregnancy T_{reg} cells. AIRE^{+}mTECs preferentially express placental and lactating mammary gland genes[30,31], providing further evidence for a role of these cells in pregnancy. In line with these studies, we now show that T_{reg} cells from pregnant, but not from non-pregnant, female mice home to the placenta where they clonally expand and can prevent miscarriages; all of these mechanisms are dependent on RANK expression in mTECs.

Human pregnancy is associated with progressive insulin resistance that, if not compensated, can manifest as overt gestational diabetes[32]—a state that, although transitory, considerably increases the risk for both mother and child to develop glucose intolerance and diabetes[33,34]. The molecular and cellular bases of gestational diabetes remain largely unknown. Our data uncover a connection between the sex-hormone- and RANK-regulated rewiring of the thymic epithelial environment, thymic T_{reg} cell expansion in pregnancy and miscarriages. Notably, RANK-regulated rewiring of the thymus is required to maintain, through VAT T_{reg} cells, glucose homeostasis in the pregnant mother. We therefore provide molecular insights into gestational diabetes and show that sex hormones, RANK signalling in the thymic epithelium and natural T_{reg} cells are a central mechanism for the integration of hormonal, immune and metabolic maternal adaptations in pregnancy.

Methods

Mice

Rank conditional mice (*Rank* ^{flox}) were generated in our laboratory and have been previously described[35]. We were given the following mouse strains: *Foxn1* ^{cre} mice[36] (G. A. Holländer), *Foxp3* ^{GFP} reporter mice[37] (A. Rudensky) and *K5* ^{cre} mice[38] (J. Takeda). *Rag2* $^{-/-}$ mice were obtained from our in-house stock and *MRL/lpr* mice were purchased from Jackson Laboratories. For fetal thymic organ culture experiments and allogeneic crosses, BALB/cJ wild-type in-house mice were used. Except where stated otherwise, all other mouse experimental studies were performed on mice that were extensively backcrossed to the C57BL/6J background and only young (7–17-week-old) age-matched littermate female mice were used for experimentation. Mice were allocated to experimental groups based on their genotype and randomized within the given sex- and age-matched group. Given that our mice were inbred and matched for age and sex, we assumed similar variance between the

different experimental groups. No statistical methods were used to predetermine sample size. We always used as many mice per group as possible in an attempt to minimize type-I and type-II errors. Critical experiments have high *n* numbers and were repeated multiple times. All sample sizes are indicated in the figure legends. Investigators were not blinded to allocation during experiments. For most studies (pregnancy studies and offspring studies) this was important, as we wanted to co-cage cohorts to reduce other variables (microbiota, matings to the same breeder, and so on). Genotyping was performed by PCR on genomic DNA and re-confirmed at the experimental end point, minimizing any potential bias during data collection. Housing conditions were: ambient temperature of 22 °C ± 1 °C; humidity of 55% +/-5% and a light/dark cycle of 14 h:10 h (light summertime, 07:00–21:00; light wintertime, 06:00–20:00). Images of mice shown in the figures were taken by M.P. in our animal facility. All animal experiments were performed following the principles of the 3Rs, in accordance with the Austrian Animal Experiments Acts and valid project licenses, which were approved and regularly controlled by the Austrian Federal Ministry of Education, Science and Research, and monitored by the institutional IMBA Ethics and Biosafety department.

Timed pregnancy studies

To exclude the potential effects of *Rank* deletion in the fetus, $Rank^{WT}$ and $Rank^{\Delta Foxn1}$ female littermates were co-caged and crossed to the same wild-type syngeneic C57BL/6J male breeder, resulting in RANK-sufficient fetuses with a comparable genetic background. Syngeneic pregnancies allowed us to better assess hormone-regulated T_{reg} cells in pregnancy. For comparison, an allogeneic pregnancy study was set up; in this case, $Rank^{WT}$ and $Rank^{\Delta Foxn1}$ female littermates were also co-caged and crossed to the same wild-type BALB/cJ male breeder. All breeding experiments were setup in the afternoon and the presence of a vaginal plug was checked daily. On the morning of plug detection—considered E0.5—females were separated from the male breeder. At the embryological day of the experimental end point, pregnant females were euthanized and all placenta–fetus units in the uterus were macroscopically evaluated for the presence of viable or resorbed fetuses. Prevalence of fetal loss is presented as a percentage of pregnant mice showing any (at least one) fetal resorption event (detected from E12.5 to E18.5); the statistical analysis of prevalence was performed with a two-tailed χ^2 test using the raw data (number of pregnant females with and without resorptions). To detect fetal macrosomia, fetuses were collected at E17.5 for measurement of their body weight using a sensitive scale. Sex genotyping of the fetuses was performed by PCR on genomic DNA using male-specific primers: Sry1, TCATGAGACTGCCAACCACAG; Sry2, CATGACCACCACCACCACCAA. Moreover, at each pregnancy end point the maternal blood, thymus, spleen, para-aortic lymph nodes, pancreas, gonadal (peri-uterine) visceral adipose tissue, lung, kidneys and placentas were collected for FACS, histological and ELISA analyses.

Flow cytometry

T cells from the thymus, spleen, lymph nodes and placenta were recovered by mechanical disruption of isolated tissues. For quantification of T_{reg} cells and macrophages in the gonadal VAT (peri-uterine for females and epididymal for males) was dissected, weighed and disaggregated (up to 0.5 g) in a gentle MACS Dissociator (Miltenyi Biotec) using an

adipose tissue dissociation kit optimized for a high yield of viable cells and preservation of cell-surface markers (Miltenyi Biotec). Dissociation of lungs and kidney tissues for FACS analysis was achieved by incubation in DMEM containing collagenase type IV and DNase I (both from Worthington Biochemical) in the gentle MACS Dissociator with heat. After digestion, samples were treated with red-blood-cell lysis buffer before staining. Single-cell suspensions were immunostained for 30 min at 4 °C in FACS buffer (PBS, 2% FCS, 2 mM EDTA). Before staining, Fc receptors were blocked with anti-CD16/32 antibodies (BD Pharmingen, 1:100) and dead cells were labelled using a fluorescently labelled and fixable viability dye (eBioscience, 1:1,000). For flow cytometry, directly labelled antibodies against CD45 (30-F11, 1:800), TCRβ (clone H57-597, 1:200), CD4 (RM4-5, 1:400), CD8α (53-6.7, 1:250), CD25 (PC61, 1:200), CD44 (IM7, 1:200), KI-67 (16A, 1:100), CCR9 (CW-1.2, 1:150), CD69 (H1.2F3, 1:150), CD11b (M1/70, 1:250), ST2 (DIH9, 1:200), GITR (DTA-1, 1:150), F4/80 (BM8, 1:300), CD11c (N418, 1:250), CD301 (LOM-14, 1:100), Ly6G (1A8, 1:300), neuropilin-1 (3E12, 1:150), Helios (22F6, 1:100) (all from Biolegend), and CCR7 (4B12, 1:150), active CASP3 (C92-605, 20 μl per sample), CTLA-4 (UC10-4F10-11, 1:150), Vβ 8.1 and Vβ 8.2 TCRs (MR5-2, 1:150), Vα 8.3 TCRs (KT50, 1:150) (all from BD Biosciences), as well as FOXP3 (FJK-16s, eBioscience, 1:100) were used. A list of all antibodies, including clones, catalogue numbers, companies and dilutions used is provided in the Reporting Summary. T_{reg} cells of thymic origin were defined as $CD4^{+}FOXP3^{+}$ cells that co-express high levels of neuropilin-1[10,39] and Helios[13]. Intracellular staining for FOXP3, Helios, KI-67 and active CASP3 were carried out using the FOXP3/Transcription Factor Staining kit (eBioscience). Data were acquired using a multi-colour flow cytometer (FACSCanto or LSR Fortessa, BD) equipped with FACSDiva software (BD). Sorting of cells was performed using a AriaIII cell sorter (BD Bioscience). Data analysis was performed using FlowJo v.10.0.0 software (TreeStar). For FACS analysis and sorting only viable cells (LIVE/DEAD Fixable dye-negative cells) were considered. Absolute splenocyte and thymocyte numbers were determined using a FACS LSR Fortessa flow cytometer equipped with a BD High Throughput Sampler for 96 wells, which allows counting of cells in a fix volume, and subsequent extrapolation for the total sample volume.

Ovariectomy and hormonal treatment

For hormonal studies in females, bilateral ovariectomy was performed under ketamine/xylazine anaesthesia through a small abdominal incision to open the peritoneal cavity[40]. Ovaries including the surrounding adipose tissue were excised. The sham surgery was only the abdominal incision. Mice were allowed to recover for 3–4 weeks before hormonal treatment. For hormonal treatment, anaesthetized female mice were implanted subcutaneously on the left flank—then moved to the interscapular region to avoid scratching and potential loss of the implant at the incision point—with slow-release pellets containing the progesterone derivative medroxyprogesterone acetate (MPA; 50 mg per pellet, 90-day release; Innovative Research of America). Oestrogen (17β-oestradiol, Sigma) was dissolved in sesame oil and was administrated subcutaneously (10 μg kg^{-1}), either alone or in combination with MPA pellets (same dose and implantation as the single treatment). Progesterone was delivered subcutaneously by daily injections (450 μg per mouse, Sigma) or by implantation of a progesterone-releasing pellet (50 mg per pellet, 21-day release, Innovative Research of America). Control mice for pellet implantation were treated with

sham surgery; controls for subcutaneous hormone injections were treated with only vehicle. We also tested placebo pellets as controls (15 mg per pellet, 21-day release, Innovative Research of America); neither the placebo pellet nor sham surgery had any overt effects on T_{reg} cell numbers when compared to untreated mice. Hormonal treatment lasted for 5 or 7 days; thereafter mice were euthanized and analysed for qPCR, expansion of T_{reg} cells and thymic alterations.

Adoptive T_{reg} cell transfer

To isolate viable bona fide FOXP3$^+$$T_{reg}$ cells, *Rank* ^{WT} and *Rank* $^{\Delta Foxn1}$ animals were crossed to *Foxp3* $^{GFP/GFP}$ reporter mice to allow sorting of T_{reg} cells based on GFP expression. Three adoptive T_{reg} cell transfer models were set up with different aims, as described below.

Tracking transplanted T_{reg} cells

To track transplanted T_{reg} cells, recipient early pregnant (E3.5–E5.5) *Rank* ^{WT} females (no *Foxp3* ^{GFP} transgene) were intravenously inoculated with 3×10^5 sorted purified CD4$^+$FOXP3–GFP$^+$neuropilin-1^{high} T_{reg} cells isolated and pooled from spleen, lymph nodes and thymus of E6.5–E8.5 *Rank* ^{WT} *Foxp3* $^{GFP/GFP}$ pregnant donors. Recipients were euthanized 5 days after transfer to determine the relative percentage of FOXP3–GPF$^+$ Transplanted T_{reg} cells in different organs (thymus, spleen, lymph nodes, VAT and placentas) using FACS analysis.

Determination of the tissue homing capacities of different T cells

To determine which cell type migrates to the placenta, wild-type female mice were used as donors as well as recipients. As wild-type mice carried no *Foxp3* ^{GFP} transgene, T_{reg} cells were sorted as CD4$^+$CD25$^+$CD45RB^{low} and conventional CD4$^+$T cells as CD4$^+$CD25$^+$CD45RB^{high} cells. T_{reg} cells from thymic origin (defined as neuropilin-1^{high}), T_{reg} cells from non-thymic origin (defined as neuropilin-1^{low}) as well as conventional T cells were sorted and pooled from spleen, lymph nodes and thymus of non-pregnant and pregnant (E8.5–E9.5) donors and transferred (intravenous inoculation, 1×10^5) into early pregnant recipients (E0.5–E2.5). Thymic T_{reg} cells (CD4$^+$CD25$^+$CD45RB^{low}neuropilin-1^{high}) were also transplanted into non-pregnant wild-type female mice. Vehicle-control pregnant females received only PBS. Recipient mice were euthanized 15 days after transfer (E15.5–E17.5) for FACS analysis of T_{reg} cell numbers and percentages in thymus, spleen and placentas.

Phenotypic rescue experiments

For phenotypic rescue experiments, non-pregnant *Rank* ^{WT} *Foxp3* $^{GFP/GFP}$ as well as E7.5–E9.5 *Rank* ^{WT} *Foxp3* $^{GFP/GFP}$ and *Rank* $^{\Delta Foxn1}$ *Foxp3* $^{GFP/GFP}$ dams were used as T_{reg} cell donors. T_{reg} cells of thymic origin were FACS-sorted and pooled from the thymus, lymph nodes and spleen as CD4$^+$FOXP3–GFP$^+$neuropilin-1^{high} T cells. Then, 1×10^5 sorted T_{reg} cells were transferred intravenously into the tail veins of E0.5–E2.5 *Rank* ^{WT} *Foxp3* $^{GFP/GFP}$ and *Rank* $^{\Delta Foxn1}$ *Foxp3* $^{GFP/GFP}$ pregnant recipient females. Vehicle-control pregnant females received only PBS on days E0.5–E2.5. To assess rescue of fetal resorption, recipient pregnant mice were euthanized on day E12.5. To assess T_{reg} cell numbers in the placenta,

recipient mice were euthanized on days E12.5 and E16.5. To assess rescue of metabolic parameters, an oral glucose-tolerance test was performed on day E16.5. Rescue of fetal macrosomia, as well as inflammation, adipocyte size and T_{reg} cell numbers in the visceral adipose tissue, was determined at E17.5. In all adoptive transfer experiments, pregnancies were from crosses to syngeneic C57BL/6J male mice and sorting of T_{reg} cells and T cells was performed after exclusion of dead cells (viability dye-negative).

Histology and immunohistochemistry

For histological analysis of the cortico-medullary organization of the thymus, 2.5-μm paraffin-sections and 5-μm cryosections were stained with haematoxylin and eosin (H&E) or assayed by immunofluorescence for K5 expression (medullary marker; Poly19055, Biolegend) and counterstained with DAPI. Slides were then scanned on a Mirax Scanner (Zeiss) and the thymic medulla area/total thymus area (expressed as a percentage) was quantified using the Fiji software (ImageJ v.1.49b). For histological analysis of mouse placentas, dissected placenta–fetus units were fixed in 4% paraformaldehyde and embedded in paraffin after dehydration. Cross-sections (2–3 μm thick) were stained with H&E and histologically examined independently by two certified pathologists. For quantification of pancreatic β-islets and white adipocyte size during pregnancy, pancreata and gonadal (peri-uterine) white adipose tissue from pregnant and non-pregnant control littermate female mice were fixed in 4% paraformaldehyde, paraffin embedded and micro-sectioned (2–3 μm thick) at 2 distal sites. Individual adipocyte and β-islets sizes as well as total pancreas areas were quantified using an automated image analysis software (Definiens Tissue Studio v.4.4.3 and Definiens Developer v.2.7; both from Definiens). An algorithm was developed to identify, categorize and measure the area of the white adipocytes as well as β-islets and the exocrine pancreas, based on morphology and intensity of the H&E staining and under the guidance of a pathologist. The validity of the analysis was manually inspected for each slide and incorrect delimitations were manually adjusted if necessary (Extended Data Fig. 5p). Detection of macrophages in the adipose tissue of non-pregnant and E17.5 pregnant females was performed using the automated staining platform Leica BOND-III System (Leica Biosystems). In brief, 2-μm thick visceral (gonadal, peri-uterine) adipose tissue paraffin sections were deparaffinized by Leica Dewax solution (AR9222) and rehydrated before epitope retrieval using Leica epitope retrieval solution 1 (AR9961) for 20 min. Sections were blocked 1 h in PBS 1% BSA and 5% rabbit serum (R9133-5, Sigma Aldrich) and incubated for 1 h with anti-F4/80 primary antibody (MCA497G, Biorad, 1:100) diluted in Leica primary antibody diluent. Slides were then incubated with biotinylated secondary rabbit anti-rat antibodies (ab6733, Abcam), diluted 1:500 in Leica primary antibody diluent, for 30 min before detection using the Leica Bond Intense R Detection system (DS9263). Staining of $FOXP3^{+}T_{reg}$ cells in mouse pancreas cross-sections was performed manually using anti-FOXP3 primary (ab54501, 1:1,000) and goat anti-rabbit IgG (E0432, 1:500, DAKO) antibodies, following routine immunohistochemistry procedures. All sections were counterstained with Harris haematoxylin (6765002, Thermo Fischer) and subsequently dehydrated in a Microm HMS 740 slide stainer. Quantification of $F4/80^{+}$ and $FOXP3^{+}$ cells was automatically performed using the Definiens Tissue Studio software v.4.4.3 (Definiens), under the guidance of a pathologist who validated the staining using positive and negative control slides. Every cell (detected by nuclear DAPI staining) in the section was classified as

positively or negatively stained. The quantification of F4/80$^+$ cells is presented as relative to other cells; that is, (number of positive nuclei/positive + negative nuclei) × 100; the quantification of FOXP3$^+$ cells in the pancreas is presented relative to the tissue area (β-islets or exocrine pancreas), determined automatically by the software. All slides were scanned on a Mirax Scanner (Zeiss) and representative images of thymic, placental, gonadal white adipose tissue and pancreas cross-sections were acquired using the Panoramic Viewer Software v.1.15.4 (3DHistech Ltd).

Immunofluorescence of thymic cross-sections

Thymi were snap-frozen in OCT and 5 μm cryosections were prepared, air-dried and subsequently fixed in ice-cold acetone (−20 °C for 10 min). Slides were briefly blocked in 1% BSA in PBS and stained for 45 min at room temperature with the following antibodies: anti-CD4 AlexaFluor647 (clone RM4-5, Biolegend, 1:200), anti-CD8 biotin (53-6.7, eBioscience, 1:200), anti-DEC205 FITC (NLDC-145, Abcam, 1:100), anti-CD40 biotin (3/23, BD Bioscience, 1:100), anti-K5 (Poly19055, Biolegend, 1:2,000) and anti-AIRE AlexaFluor488 (5H12, eBioscience, 1:100). If primary antibodies were not directly conjugated to a fluorophore, AlexaFluor-conjugated streptavidin or secondary antibodies (Invitrogen, 1:1,000) were used for detection. DAPI was used for nuclear counterstaining. Confocal images were obtained using a Zeiss LSM 780 and Zeiss LSM 510 microscopes. For RANK staining, biotinylated anti-RANK antibodies (BAF692; R&D systems; 1:50, overnight incubation) and the TSA Fluorescence System (PerkinElmer) were used according to the manufacturer's protocol. For quantification of AIRE$^+$ medullary thymic epithelial cells (mTECs), 4–7 different medullary areas (identified by K5$^+$ staining) were quantified per mouse. The total number of AIRE$^+$ cells (manually annotated) was related to the thymic medullary area (automatically calculated using Fiji v.1.49b software). The amount of AIRE$^+$ mTECs is presented in the figures as a fold change after normalization to the average value of the control mouse group for each experiment. We verified that *Rank* heterozygosity (*Rank* $^{floxed/wt}$ *K5* $^{cre/wt}$) did not alter mTEC development, excluding Cre-dependent effects or haploinsufficiency (Extended Data Fig. 1f, g).

Quantitative PCR

Total RNA was extracted from human placenta samples of pregnant women at delivery (central part, maternal side) as well as from the gonadal VAT, whole thymi or from the thymic stroma-enriched fraction of pregnant, non-pregnant and hormone-treated female mice. Thymic stroma enrichment was obtained by enzymatic disaggregation with 0.05% (w/v) of Liberase TH and 100 U ml^{-1} of DNase I as previously described[41], followed by depletion of CD45$^+$ haematopoietic cells using magnetic microbeads (Miltenyi Biotec). For a more-representative analysis of large tissues (that is, gonadal white adipose mouse tissue and human placenta samples), total RNA was independently extracted and analysed from 3 distal sites. RNA extraction was performed using the RNAeasy Mini Kit (Qiagen) and included DNase I digestion to avoid potential DNA contamination. Then, 1 μg of total RNA was reverse transcribed using iScript cDNA Synthesis Kit (BioRad). Gene-expression levels were quantified by real-time quantitative PCR (iCycler iQ BioRad) using the iQ SYBR Green Supermix from BioRad and normalized to *Actb* or *Pum1* housekeeping genes. mRNA fold changes were calculated using the $\Delta\Delta C_t$ method.

The following primers were used for mouse genes: *Aire* forward, CTCTGCTAGTCACGACCCTG; *Aire* reverse, AGAGAAGGGTGGTGTCTCGG. *Rank* forward, CCCAGGAGAGGCATTATGAG; *Rank* reverse, CACACACTGTCGGAGGTAGG. *Actb* forward, CGGTTCCGATGCCCTGAGGCTCTT; *Actb* reverse, CGTCACACTTCATGATGGAATTGA. *Pum1* forward, TGTGGTCCAGAAGATGATCG; *Pum1* reverse, GGATGTGCTTGCCATAGGTG. *Il6* forward, CAAAGCCAGAGTCCTTCAGAG; *Il6* reverse, AGCATTGGAAATTGGGGTAG. *Tnf* forward, TCTTCTCATTCCTGCTTGTGG; *Tnf* reverse, ATGAGAGGGAGGCCATTTG. *Ccl2* forward, CAGCAGGTGTCCCAAAGAAG; *Ccl2* reverse, TTCCGATCCAGGTTTTTAAT. *Glut4* forward, CTGTCGCTGGTTTCTCCAAC; *Glut4* reverse, CGGCAAATAGAAGGAAGACG. *Pgr* forward, ACAGCGCTTCTACCAACTCAC; *Pgr* reverse, CAACTGGGCAGCAATAACTTC.

The following primers were used for human genes: *PUM1* forward, CGGTCGTCCTGAGGATAAAA; *PUM1* reverse, CGTACGTGAGGCGTGAGTAA. *CD4* forward, TTTTCATTGGGCTAGGCATC; *CD4* reverse, ACTGGCAGGTCTTCTTCTCAC; *FOXP3* forward, AAGCAGCGGACACTCAATG; *FOXP3* reverse, TGTGCAGACTCAGGTTGTGG.

RNA sequencing

QuantSeq analysis of VAT—Using the RNAeasy Mini Kit (Qiagen), total RNA was extracted from the gonadal VAT of dams at E17.5 treated according to our T_{reg}-cell adoptive transfer protocol. Tissues from four independent dams were analysed for each of the three pregnant mouse cohorts: vehicle-treated $Rank^{WT}$ $Foxp3^{GFP/GFP}$ as well as vehicle-treated $Rank^{\Delta Foxn1}$ $Foxp3^{GFP/GFP}$ dams and pregnancy thymic-T_{reg}-cell-treated (hereafter, pregnancy tT_{reg}-cell-treated) $Rank^{\Delta Foxn1}$ $Foxp3^{GFP/GFP}$ dams. After RNA extraction, RNA quantification and quality control were performed with the Agilent RNA 6000 Nano Kit on the bioanalyser. Thereafter, 200 ng of total isolated RNA was used for library preparation using the Lexogen QuantSeq 3′ mRNA-Seq Library Prep Kit FWD for Illumina. Preparations were performed according to the manufacturer's recommendations. The quality controls of the final libraries were composed of a fragment analyser run to determine the average size, followed by qPCR to quantify library concentration. Libraries were pooled at an equimolar ratio and sequenced on an Illumina HiSeq 2500 instrument using the single-read 50-read mode. 3′ RNA-sequencing (Quantseq) reads were prepared for analysis by removing adaptor contamination, poly(A) read through and low-quality tails using bbmap v.36.92. Thereafter reads were aligned to the *Mus musculus* genome mm10 using TopHat v.2.1.1 (GTF annotation file mm10, RefSeq from UCSC, 2015/02, protein-coding genes). Reads in genes were counted with htseq-count v.0.6.1. Differential expression analysis was performed with DESeq2 v.1.16.1. Raw expression counts were converted to counts per million (CPM) using edgeR v3.18.1. For gene set enrichment analyses (GSEA), genes with very low expression levels were filtered out by setting an expression threshold of CPM > 1 in at least 2 samples. GSEA was performed using GSEA v.3.0 and gene signatures from MSigDB v.6.1.

Smart-Seq2 analysis of tissue T_{reg} cells—For transcriptome analysis of pregnancy-associated T_{reg} cells, placentas, thymi, spleen and VAT from *Rank* ^{WT} *Foxp3* $^{GFP/GFP}$ and *Rank* $^{\Delta Foxn1}$ *Foxp3* $^{GFP/GFP}$ pregnant females were isolated at E17.5. To recover thymocytes, thymi were mechanically disrupted. Isolated placentas and VAT (peri-uterine) were enzymatically digested in DMEM medium containing collagenase IV (1 mg ml^{-1}) and DNase I (0.1 mg ml^{-1}) (both from Worthington), shaking at 37 °C for 40 min at 100 rpm, or using an adipose tissue dissociation kit and a gentle MACS Dissociator (Miltenyi Biotec), respectively. After digestion, samples were put on ice and washed twice with DMEM containing 10 mM EDTA and 10% FCS to stop the enzymatic digestion and subsequently stained for FACS as described above. Cell sorting was performed on an AriaIII cell sorter (BD Bioscience) after excluding dead cells and doublets, and gating for low side scatter and $CD45^+$ haematopoietic cells (gating strategy is shown in Supplementary Data 1). Equal numbers of T_{reg} cells (280 cells) were sorted as $CD45^+CD8^-CD4^+$FOXP3–GFP $^+$neuropilin-1^{high} cells from the thymus and placenta (both samples from the same female). To increase robustness, the 280 placental T_{reg} cells were purified from 5 individual placentas per pregnant female (56 T_{reg} cells per placenta). In a separate experiment with different pregnant mice than those used for thymus and placenta analysis, VAT T_{reg} cells (20–30 cells) and splenic T_{reg} cells (150 cells) were sorted (both samples from the same female). In all cases, cells were sorted directly into a cell lysis buffer consisting of a 0.2% (v/v) Triton X-100 solution and an RNase inhibitor (TaKaRa Bio Group). For the generation of full-length cDNA, the Smart-seq2 protocol[42] was used. Subsequent library preparation from the amplified cDNA was performed using the Nextera XT DNA library prep kit (Illumina). Expression profiling libraries were sequenced on a HiSeq3000 instrument (Illumina) in 50-base-pair, single-end mode. Base calls, provided by the real-time analysis software (RTA v.2.7.3 and v.2.7.7, Illumina), were subsequently converted into multiplexed, unaligned BAM format before demultiplexing into sample-specific, unaligned BAM files. For raw data processing off the instruments, custom programs, based on Picard tools (v.2.19.2, https://broadinstitute.github.io/picard), were used. Next-generation sequencing (NGS) reads were mapped to the Genome Reference Consortium GRCm38 assembly using ‘Spliced Transcripts Alignment to a Reference’ (STAR, v.2.7.5a)[43] using the ‘basic’ Ensembl transcript annotation from version e96 (April 2019) as reference transcriptome. As the mm10 assembly of the UCSC Genome Browser was preferred for downstream data processing with Bioconductor packages (v.3.11, https://bioconductor.org/packages), Ensembl transcript annotation had to be adjusted to UCSC Genome Browser sequence region names. STAR was run with options recommended by the ENCODE project. Aligned NGS reads overlapping Ensembl transcript features were counted with the summarizeOverlaps function of the Bioconductor GenomicAlignments package. Transcript-level counts were aggregated to gene-level counts and the Bioconductor DESeq2[44] package was used to test for differential expression based on a model using the negative binomial distribution. An initial exploratory analysis included principal component analysis, multi-dimensional scaling, sample distance and expression heat map plots, all annotated with variables used in the expression modelling (ggplot2[45], Bioconductor ComplexHeatmap), as well as volcano plots (Bioconductor EnhancedVolcano). On the basis of poor sample quality in principal component analysis plots and sample distance heat maps at the exploratory analysis stage, three low-input samples were excluded from the differential expression

analysis of tissue T_{reg} cells. The samples included one thymic T_{reg} cell sample from a pregnant *Rank* ^{WT} mouse (GTT13_T_S13943) and two placental T_{reg} cell samples, one from a *Rank* ^{WT} pregnant female (GTT31_P_S13938) and one from a *Rank* $^{\Delta Foxn1}$ pregnant female (GTT16_P_S13933) (all samples, including the excluded ones, have been deposited in the NCBI GEO). Resulting gene lists were annotated, filtered for significantly differentially up- and downregulated genes and independently subjected to GSEA (GSEAPreranked, using GSEA v.3.0 and gene signatures from MSigDB v.6.2). The TCR repertoire was estimated with the MiXCR[46] software (v.3.0.13) and the immunarch (v.0.6.5) R package from GitHub (https://github.com/immunomind/immunarch). To obtain a sensible number of NGS reads from conventional, poly(A)-primed mRNA sequencing, reads of all replicate samples were pooled, aligned to immune genes and assembled into clones and clonotypes via MiXCR.

Fetal thymus organ culture—For fetal thymus organ cultures (FTOCs), day E16 thymic lobes from wild-type pregnant females were cultured for 7 days in DMEM, then cultured in the presence of 100 ng ml^{-1} soluble recombinant mouse RANKL (Peprotech) and/or 1,000 ng ml^{-1} osteoprotegerin (R&D systems) for an additional 4 days. Fetal thymic lobes were then mechanically disaggregated and stained with antibodies to detect CD4 (RM4-5, Biolegend), CD8 (53-6.7, eBioscience) and FOXP3 (FJK-16s, eBioscience, using the FOXP3 intracellular staining buffer). FACS data were analysed using a FACSFortessa BD.

Detection of autoantibodies—For the detection of autoantibodies, indirect immunofluorescence on *Rag2* $^{-/-}$ tissue sections was performed as described previously[47]. In brief, 5-μm cryostat sections from several organs of *Rag2* $^{-/-}$ mice were incubated with 1/40 dilutions of sera obtained from pregnant females, followed by detection with AlexaFluor555-labelled anti-mouse IgG secondary antibodies (Invitrogen, 1:1,000). Serum from antibody-deficient (*Rag2* $^{-/-}$) and autoimmune-prone (*Mrl/lrp*) females were used as positive and negative controls, respectively. DAPI was used for nuclear staining. Slides were examined and scored in a blinded fashion, and representative images were acquired using the Panoramic Viewer Software v.1.15.4 (3DHistech). Anti-dsDNA autoantibodies were detected by ELISA according to the manufacturer's protocol (Alpha Diagnostic).

T_{reg} cells in vitro suppression assays—For comparing the suppression capacity of T_{reg} cells from spleen and lymph nodes, $CD4^+CD25^+FOXP3^{GFP}$ neuropilin-1^{high} T_{reg} cells were sorted from the freshly isolated spleen and lymph nodes of *Rank* ^{WT} *Foxp3* $^{GFP/GFP}$ and *Rank* $^{\Delta Foxn1}$ *Foxp3* $^{GFP/GFP}$ non-pregnant and E12.5–E14.5 pregnant female mice using an AriaIII cell sorter (BD Bioscience). To compare *Rank* ^{WT} *Foxp3* $^{GFP/GFP}$ and *Rank* $^{\Delta Foxn1}$ *Foxp3* $^{GFP/GFP}$ T_{reg} cell populations against a common responder, purified FOXP3-GFP^+T_{reg} cells (2.5×10^4) were co-cultured at different ratios (from 1:1 to 1:32) with a pool of naive $CD4^+CD25^-FOXP3–GFP^-$ effector T cells that were similarly sorted from $n = 3–4$ *Rank* ^{WT} *Foxp3* $^{GFP/GFP}$ donors and subsequently stained with a CellTrace Cell Proliferation Kit (violet, 5 μmol l^{-1}, Life Technologies), according to the manufacturer's instructions. Effector T cells from non-pregnant *Rank* ^{WT} *Foxp3* $^{GFP/GFP}$ donors were used in co-cultures with T_{reg} cells from non-pregnant *Rank* ^{WT} *Foxp3* $^{GFP/GFP}$ and *Rank* $^{\Delta Foxn1}$ *Foxp3* $^{GFP/GFP}$ mice. Similarly, effector T cells isolated from pregnant *Rank* ^{WT} *Foxp3* $^{GFP/GFP}$ donors were

used to test the suppression capacity of pregnancy-associated *Rank* ^{WT} *Foxp* $^{3GFP/GFP}$ and *Rank* $^{\Delta Foxn1}$ *Foxp3* $^{GFP/GFP}$ T_{reg} cells. The proliferation of $CD4^+$T effector cells was induced by incubation in 200 µl of IMDM containing 10% FCS, in a 96-round-well plate, in the presence of soluble anti-CD3 antibodies (0.25 µg ml^{-1}) as well as $CD11c^+$ dendritic cells (5×10^3) isolated from enzymatically digested spleens of wild-type C57BL/6J age-matched and non-pregnant female mice using MACS beads (Miltenyi Biotec). After 3 days of stimulation, the relative percentage of proliferating $CD4^+GFP^-$ effector T cells was determined based on CellTrace Violet dilution data collected with a LSR II flow cytometer (BD Biosciences) and analysed using FlowJo v.10.0.0 software (Tree Star). Percentage of T_{reg} cell suppression was calculated by comparing the proliferation of the effector T cells co-plated with T_{reg} cells at each ratio to the proliferation of effector T cells plated without T_{reg} cells (0:1 ratio).

Metabolic studies

Diet and husbandry—For metabolic studies during pregnancy, pregnant *Rank* ^{WT} and *Rank* $^{\Delta Foxn1}$ female mice as well their non-pregnant control littermates were fed normal chow. *Rank* ^{WT} and *Rank* $^{\Delta Foxn1}$ female mice were co-caged before and during pregnancy to minimize the effects of the microbiota on metabolic parameters. Their offspring were fed normal chow from weaning age until 80 days of age, after which they were fed a HFD (60% kcal% fat, Research Diets, D12492i) for up to 12 weeks. Offspring pups were weighted periodically starting from postnatal day 1 until weaning age. After weaning, tail blood glucose samples and body weight measurements of the offspring were obtained weekly, for mice fed normal chow or HFD. To discard milk or other mother-related effects, *Rank* ^{WT} and *Rank* $^{\Delta Foxn1}$ dams were interchanged to nurture each other litters, from postnatal day 1 until weaning age. After weaning, the offspring from *Rank* ^{WT} and *Rank* $^{\Delta Foxn1}$ were co-caged to minimize possible effects of the microbiota and/or cage. For analysis of long-term transgenerational effects on fat tissues, male and female offspring were kept on a normal chow diet for up to 17 months. For metabolic studies in non-pregnancy conditions, non-pregnant *Rank* ^{WT} and *Rank* $^{\Delta Foxn1}$ females were fed a HFD for 7 weeks, after which their glucose tolerance and adipose tissue were characterized.

Glucose and insulin measurements—All glucose-tolerance tests (GTT) were performed orally. For oral glucose-tolerance tests, mice were fasted for 16 h (15:00–07:00) and were then administrated 2 mg glucose per g body mass by oral gavage. Glucose values were measured using glucometers from blood samples taken by tail nick at 0, 5, 15, 30, 60 and 120 min after glucose ingestion. The area under the GTT curve was calculated for each mouse using GraphPad Prism v.7.0c (GraphPad Software). Fed and fasting glucose measurements were performed from blood tail samples or serum (OneTouch UltraEasy, according to the manufacturer's instructions); insulin levels were measured from serum by ELISA (mouse ultrasensitive insulin ELISA, Alpco). For each litter of dams, offspring, as well as non-pregnant females, blood samples were taken the same day and at the same time for all genotypes of interest. The glucose uptake capacity of the adipose tissue was determined using 2-deoxyglucose and the bioluminescent Glu-Uptake Glo Assay (Promega). In brief, small pieces (around 4–9 mg) of VAT were incubated with 0.5 mM of 2-deoxyglucose for 15 min. For insulin-induced glucose uptake, tissues were pre-incubated for

20 min with 100 nM insulin, washed twice with PBS and then treated with 2-deoxyglucose (same time and dose). Glucose uptake values were measured using a luminometer as relative luminescence units and were normalized per mg adipose tissue.

Mass spectrometry measurements of glucose in the placental tissue— Metabolites were extracted from the E17.5 placentas of *Rank* ^{WT} and *Rank* $^{\Delta Foxn1}$ mice (around 30–40 mg) using a methanol:acetonitrile:water (2:2:1, v/v) ice-cold solvent mixture followed by subsequent rounds of snap-freezing, bead homogenization and sonication. Samples were then centrifuged at 4,000*g* for 10 min at 4 °C, the supernatants collected and transferred to another tube and evaporated to dryness in a vacuum concentrator. Extracted metabolites were resolubilized in a buffer containing 50% 20 mM ammonium acetate and 50% acetonitrile. Then, 1 µl of the sample was injected and separated using an Ulitimate U300 BioRSLC HPLC system (Dionex; Thermo Fisher Scientific), using a HILIC column (100 mm × 2.1 mm, 3.5 µm, 200 Å; Merck). Separation was carried out with a flow rate of 100 µl min^{-1} using a linear gradient of 13 min from 95% A (acetonitrile) to 45% B (10 mM ammonium acetate pH 7.5), followed by re-equilibration of the column. Eluting metabolites were analysed using a TSQ Quantiva mass spectrometer (Thermo Fisher Scientific) after electrospray ionization with single-reaction monitoring in negative ion mode using a spraying potential of 3,000 V. Glucose was quantified using the transitions *m*/*z* 239 to 179 (acetate adduct; quantifier) and *m*/*z* 179 to 119 (qualifier). Data were manually interpreted using the Xcalibur software (Thermo Fisher Scientific) and normalized per mg placental tissue.

Human data—For human studies, approval from the ethics committee of the Medical University of Vienna (EC number 1337/2016) as well as written informed consent from all participants was obtained. The study was performed in accordance with the principles of the Declaration of Helsinki. Pregnant women with gestational diabetes mellitus (GDM) and control glucose-tolerant pregnant women, older than 18 years (mean age, 34 years; with a 25th percentile of 30 years and 75th percentile of 36.25 years), carrying a singleton pregnancy, were both stratified as overweight or obese (body-mass index (BMI) ≥ 29.0 kg m^{-2}). None of the women had any pre-existing diabetes, chronic medical condition or psychiatric disease. Participants underwent a standard 75 g oral glucose-tolerance test for which venous samples were taken at time 0 (fasting overnight) and at 30, 60, 90 and 120 min after glucose ingestion and measured for glucose and insulin levels in plasma by enzymatic methods at the General Hospital in Vienna (AKH Wien). Participants undertook a first oral glucose-tolerance test at early pregnancy (≤20 gestational weeks; Fig. 4g), which is advised for obese pregnant women[48] and were retested at mid gestation (24–28 weeks) and late gestation (35–38 weeks), with similar results (data not shown). At each visit, anthropometric measurements for BMI calculations were also taken. GDM was diagnosed according to the IADPSG/WHO 2013 criteria[49,50] of fasting plasma glucose ≥ 5.1mmol l^{-1}, 1 h plasma glucose ≥ 10.0 mmol l^{-1} or 2 h plasma glucose ≥ 8.5 mmol l^{-1}. Homeostatic model assessment of insulin resistance was calculated from fasting insulin and glucose values as follows: (fasting glucose (mmol l^{-1}) × fasting insulin (pmol l^{-1}))/135. The following data from the included patients were collected: age, height, weight (before pregnancy and at birth), BMI, gender of the baby, gestational week of delivery, method of delivery as well as

complications in pregnancy, therapy of GDM, glucose control and glycaemic parameters. At delivery, samples from the cord blood (baby side) as well as samples from the centre of the placenta, at the maternal side (decidua) were collected. Cord blood samples were used to determine C-peptide levels using immunoassays. Birth weights were determined without diaper using a calibrated electronic scale. Preparations of placenta samples were performed at the same position in all cases. For FOXP3 qPCR studies, dissected placenta samples were immediately frozen and stored for later RNA analysis. Three distal placental slices (all on the maternal side) were analysed and averaged per woman. *FOXP3* mRNA transcripts were normalized to a housekeeping gene (Fig. 4i, j), but similar results were observed if normalized to *CD4* levels (Extended Data Fig. 10h). In a subsequent additional study for FOXP3 immunohistochemistry, the placenta samples were fixed in 10% neutral-buffered formalin, embedded in paraffin and micro-sectioned at 2–3 distal sites for detection of T_{reg} cells using immunohistochemical analysis, using anti-FOXP3 (ab20034, 1:200) and goat anti-rabbit (DAKO, E0432, 1:500) antibodies in the automated staining platform Leica BOND-III System (Leica Biosystems). In total 2–3 distal placental slices (all on the maternal side) were analysed per woman. Slides were scanned on a Mirax Scanner (Zeiss) and the quantification of $FOXP3^+$ cells was performed using the Definiens Tissue Studio software 4.4.3 (Definiens), under the guidance of a pathologist, who manually inspected the validity of the analysis, verifying nuclear staining and positive staining of human tonsil control slides. Every cell (nucleus) on the placenta section was quantified as negatively or positively stained. Images of the stained cross-sections were acquired using the Panoramic Viewer Software 1.15.4 (3DHistech). Of note, we had no access to fat tissue from the same female cohorts and hence could not determine T_{reg} cell numbers in fat. For the analysis of the human data (except the immunohistochemistry study), all women with GDM were matched to control glucose-tolerant women for BMI (mean ± s.d. of 33.9 ± 4.8 for control and 34.3 ± 5.0 for GDM), gestational week of delivery (mean ± s.d. of 39.5 ± 1.6 for control and 40.0 ± 1.3 for GDM) and delivery method (vaginal or caesarean section; $n = 7$ and 9 for control and $n = 6$ and 10 for GDM, respectively). Of note, the reduction in *FOXP3* transcripts in the placenta of pregnant women with GDM was observed, to a similar extent, in both vaginal and caesarean section deliveries; therefore, the T_{reg} cell reduction appears to be independent of the mode of delivery of the baby (data not shown). Among pregnant women with GDM the distribution between those receiving insulin as treatment (maximum dose of 48 IE per day) and those who had sufficient metabolic control with dietary advice was also distributed equally ($n = 8$ and 8; diet and insulin treatment, respectively). Moreover, male and female sex of the babies were equally distributed in both cohorts ($n = 8$:8 male:female per group).

Statistical analyses—Unless otherwise stated, data are shown as individual data points or as mean ± s.e.m. The numbers of mice and individuals per group used in each experiment are annotated as '*n*'. Mouse experiments shown were reproduced 2–5 independent times. Figures and statistical analyses were generated using GraphPad Prism 7.0c (GraphPad Software). Normally distributed data were analysed using unpaired two-tailed Student's *t*-tests for single comparisons, one-way ANOVAs for multiple comparisons or two-way ANOVAs for comparison of two groups over time. Ordinal and not normally distributed data (according to D'Agostino and Pearson omnibus normality tests) were analysed using

unpaired two-tailed Mann–Whitney *U*-tests for single comparisons or Kruskal–Wallis tests for multiple comparisons. Post hoc tests used for multiple comparisons are indicated in each figure legend. The sex distribution of the offspring, as well as the prevalence of resorbed fetuses and autoimmunity, were analysed using a two-tailed χ^2 test. $P \leq 0.05$ was considered to indicate statistical significance; $*P \leq 0.05$; $**P \leq 0.01$; $***P \leq 0.001$.

Extended Data

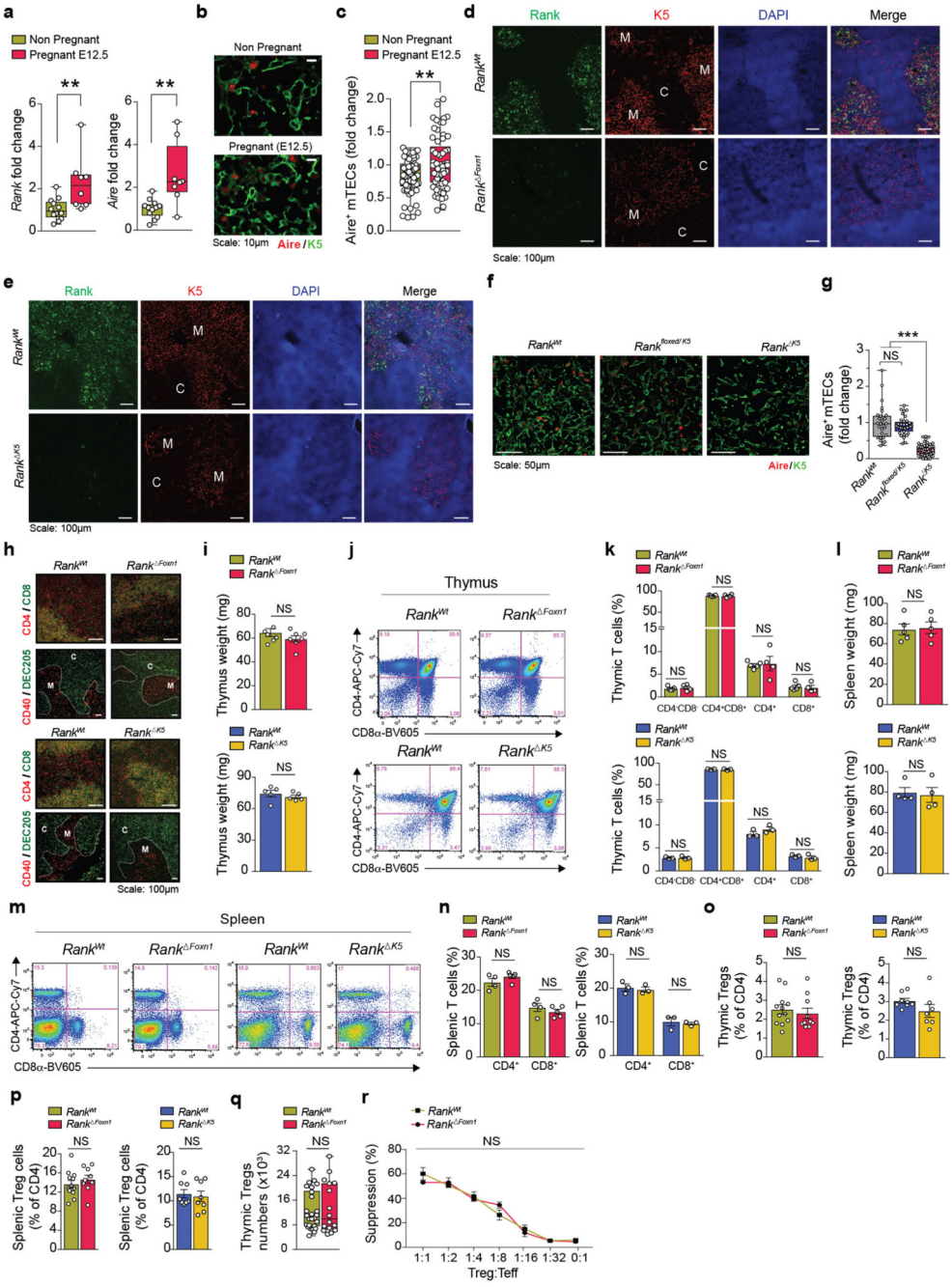

Europe PMC Funders Author Manuscripts

Extended Data Fig. 1. Characterization of non-pregnant *Rank* $^{\Delta Foxn1}$ and *Rank* $^{\Delta K5}$ conditional knockout mice.

a, qPCR analysis for relative *Rank* and *Aire* mRNA expression in the thymus of non-pregnant (N.P.; $n = 12$) and E12.5 pregnant ($n = 8$) *Rank* ^{WT} mice, normalized to non-pregnant values. Data are shown as box-and-whisker plots (from minimal to maximal values); dots represent individual mice.** $P < 0.01$. Two-tailed Student's *t*-test. **b**, **c**, Immunofluorescence staining for AIRE (red) and K5 (K5, green) in thymus cross-sections (**b**, representative of $n = 68/61$ images) and relative quantification of AIRE$^+$ mTECS in the thymic medullary regions (**c**) of non-pregnant and E12.5 pregnant *Rank* ^{WT} females ($n = 11/12$). Data are shown as box-and-whisker plots (from minimal to maximal values); dots represents individual data points (4–7 medullary fields per mouse), normalized to *Rank* ^{WT} non-pregnant values. ** $P < 0.01$. Two-tailed Student's *t*-test. **d**, **e**, Representative immunofluorescence staining for RANK (green), K5 (red), and DAPI (blue, to visualize nuclei) in thymic cross-sections of *Rank* ^{WT} and *Rank* $^{\Delta Foxn1}$ (**d**) and *Rank* ^{WT} and *Rank* $^{\Delta K5}$ (**e**) mice. Note that *Rank* expression is confined to the thymic medullary epithelium in *Rank* ^{WT} mice and is effectively ablated in *Rank* $^{\Delta Foxn1}$ as well as *Rank* $^{\Delta K5}$ mice. M, medulla; C, cortex. Images are representative of $n = 5$ mice per group. **f**, Immunofluorescence staining for AIRE (red) and K5 (green) in thymic cross-sections of *Rank* ^{WT}, *Rank* $^{flox/K5}$, and *Rank* $^{\Delta K5}$ mice. Representative of $n = 28/35/56$ images. **g**, Relative numbers of AIRE$^+$ mTECs in thymic medullary regions of *Rank* ^{WT}, *Rank* $^{flox/K5}$ and *Rank* $^{\Delta K5}$ littermates, as determined by immunofluorescence. Note that *Rank* heterozygosity and Cre expression in the thymic epithelium does not affect AIRE$^+$ mTECs numbers. Data were normalized to *Rank* ^{WT} values and are shown as box-and-whisker plots (from minimal to maximal values); dots represent individual data points. $n = 5/5/9$ (4–6 fields per mouse). *** $P < 0.001$. One-way ANOVA, Tukey's post hoc test. **h**, Organization of the thymic microenvironment. Representative immunofluorescence staining of thymic cross-sections of *Rank* ^{WT} and *Rank* $^{\Delta Foxn1}$ as well as *Rank* ^{WT} and *Rank* $^{\Delta K5}$ mice, to evaluate thymocyte distribution (top), defined by CD4 (red) and CD8 (green), as well as thymic epithelium organization (bottom), defined by CD40 (medulla, red) and DEC205 (cortex, green) expression. C, cortex; M, medulla. Representative of $n = 5$ mice per group. **i**, Thymus weights in *Rank* ^{WT} and *Rank* $^{\Delta Foxn1}$ ($n = 7$) as well as *Rank* ^{WT} and *Rank* $^{\Delta K5}$ ($n = 5$) female mice. Data are mean ± s.e.m. Two-tailed Student's *t*-test. **j**, **k**, Representative FACS blots for CD4 and/or CD8α-expressing thymocytes (**j**) and their respective percentages (**k**, mean ± s.e.m.) in the thymus of *Rank* ^{WT} and *Rank* $^{\Delta Foxn1}$ ($n = 5/4$) and *Rank* ^{WT} and *Rank* $^{\Delta K5}$ ($n = 3/3$) female mice. Two-tailed Student's *t*-test. **l**, Spleen weights of *Rank* ^{WT} and *Rank* $^{\Delta Foxn1}$ ($n = 5/5$) and *Rank* ^{WT} and *Rank* $^{\Delta K5}$ ($n = 4/4$) female mice. Data are mean ± s.e.m. Two-tailed Student's *t*-test. **m**, **n**, Representative FACS blots for CD4 and/or CD8α expression (**m**) and percentages of CD4$^+$ or CD8$^+$T cells (**n**, mean ± s.e.m.) in the spleen of *Rank* ^{WT} and *Rank* $^{\Delta Foxn1}$ ($n = 5/4$) mice as well as *Rank* ^{WT} and *Rank* $^{\Delta K5}$ ($n = 3/3$) female mice. Two-tailed Student's *t*-test. **o**, **p**, Percentages of CD4$^+$FOXP3$^+$T$_{reg}$ cells in the thymus (**o**) and spleen (**p**) of *Rank* ^{WT} and *Rank* $^{\Delta Foxn1}$ ($n = 12/9$) mice as well as *Rank* ^{WT} and *Rank* $^{\Delta K5}$ ($n = 8/7$) female mice. Data are mean ± s.e.m., determined by FACS. Two-tailed Mann–Whitney *U*-test. **q**, Total number of T$_{reg}$ cells in the thymus of *Rank* ^{WT} and *Rank* $^{\Delta Foxn1}$ ($n = 26/16$) female mice. These mice are the littermate controls of the pregnant cohorts shown in Fig. 1d. Data are shown as box-and-whisker plots

(from minimal to maximal values) and dots represent individual mice. Two-tailed Student's *t*-test. **r**, Percentage of suppression of $CD4^+$T effector cells proliferation mediated by T_{reg} cells, as determined by flow cytometry using CellTrace Violet dilution, for peripheral (pool of splenic and lymph node) T_{reg} cells isolated from *Rank* ^{WT} ($n = 4$) and *Rank* $^{\Delta Foxn1}$ ($n = 4$) female mice and co-cultured with *Rank* ^{WT} effector T cells at the indicated ratios. Data are mean ± s.e.m. Two-way ANOVA, Sidak's multiple comparisons test. All data in the figure are from young (4–12-week-old) and non-pregnant female mice.

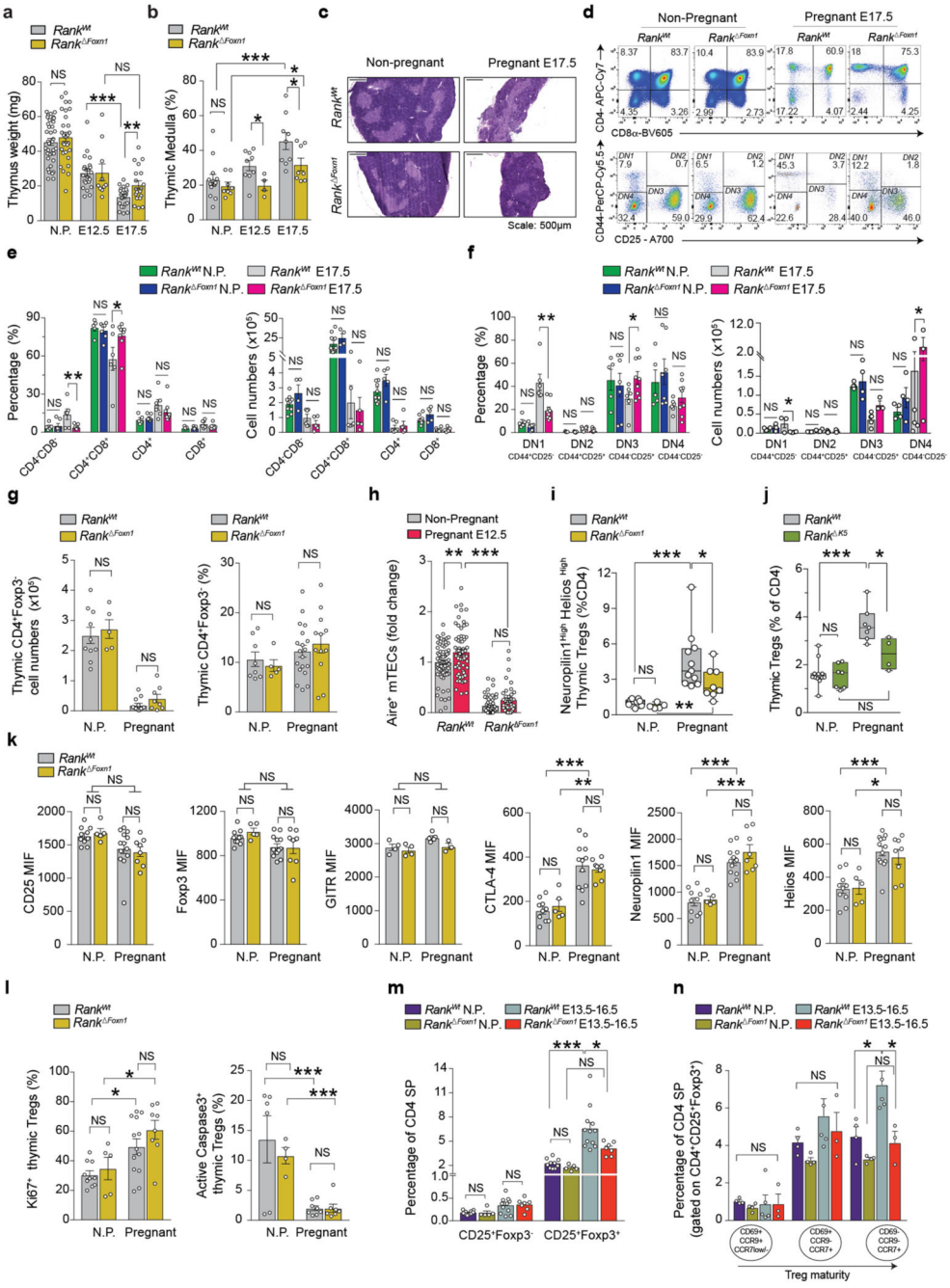

Extended Data Fig. 2. *Rank* deletion in mTECs impairs thymic adaptations and thymic T_{reg} cell expansion during pregnancy.

a, **b**, Thymus weights (**a**) and percentages (**b**) of the thymic medulla areas in non-pregnant as well as in E12.5 and E17.5 pregnant $Rank^{WT}$ and $Rank^{\Delta Foxn1}$ mice. Data are mean ± s.e.m., each dot represents an individual mouse. n = 37/22/22 and n = 29/10/19 in **a**; n = 13/9/9 and n = 8/4/8 in **b**; for the $Rank^{WT}$ and $Rank^{\Delta Foxn1}$ groups, respectively. *P < 0.05; **P < 0.01; ***P < 0.001. Two-tailed Student's t-test. Similar thymic involution defects were observed in $Rank^{\Delta K5}$ dams as compared to their $Rank^{WT}$ counterparts (data not shown). **c**, H&E-stained thymic cross-sections of non-pregnant and E17.5 pregnant $Rank^{WT}$ and $Rank^{\Delta Foxn1}$ mice. Representative of n = 13/8 and n = 9/8 (E17.5) mice. These sections as well as thymic cryo-sections stained for DAPI/K5 (data not shown) were used for the quantification of the thymic medulla expansion during pregnancy shown in **b**. **d**, Representative FACS blots for CD4 and CD8 expression (upper blots) and CD44 and CD25 expression (lower blots, gated on double negative -DN- $CD4^{-}CD8^{-}$ cells) in thymocytes of non-pregnant and E17.5 pregnant $Rank^{WT}$ and $Rank^{\Delta Foxn1}$ females. Numbers indicate percentage of cells in each quadrant. DN1, $CD44^{+}CD25^{-}$; DN2, $CD44^{+}CD25^{+}$; DN3, $CD44^{-}CD25^{+}$; DN4, $CD44^{-}CD25^{-}$. **e**, **f**, Percentages and total cell numbers of thymocyte subpopulations expressing CD4 and/or CD8 (**e**) and early developing double-negative (DN) thymocytes (as detected by CD44 and CD25 staining on $CD4^{-}CD8^{-}$ DN populations) (**f**) in the thymus of non-pregnant and E17.5 pregnant $Rank^{WT}$ and $Rank^{\Delta Foxn1}$ females. Data are mean ± s.e.m., dots represent individual mice. n = 3–10 animals per group *P < 0.05; **P < 0.01. One-way ANOVA. Similar percentage results were observed when comparing $Rank^{WT}$ and $Rank^{\Delta K5}$ dams at E18.5 (not shown). **g**, Total cell numbers and percentages of conventional single positive $CD4^{+}$ thymocytes ($FOXP3^{-}$) in the thymus of non-pregnant and E13.5–E16.5 pregnant $Rank^{WT}$ and $Rank^{\Delta Foxn1}$ females. Data are mean ± s.e.m., dots represent individual mice. n = 5–19 animals per group. Two-tailed Student's t-test. **h**, Relative quantification of $AIRE^{+}$ mTECS in the thymic medullary regions of non-pregnant and E12.5 pregnant $Rank^{WT}$ (n = 12/12) and $Rank^{\Delta Foxn1}$ (n = 13/10) mice, as determined by immunofluorescence (5–7 medullary fields per mouse). Data are mean ± s.e.m., normalized to $Rank^{WT}$ non-pregnant values. Each dot represents an individual data point. **P < 0.01; ***P < 0.001. One-way ANOVA, Tukey's post hoc test. **i**, Percentages of neuropilin-$1^{high}Helios^{high}FOXP3^{+}T_{reg}$ cells (of total $CD4^{+}$ cells) in the thymus of non-pregnant (n = 9/5) and pregnant (pool from E15.5–E17.5, n = 11/8) $Rank^{WT}$ and $Rank^{\Delta Foxn1}$ females, as determined by FACS analysis. Data are shown as box-and-whisker plots (from minimal to maximal values) and each dot represents an individual mouse. *P < 0.05; **P < 0.01; ***P < 0.001. Two-tailed Mann–Whitney U-test. **j**, Percentages of $CD4^{+}FOXP3^{+}T_{reg}$ cells (of total $CD4^{+}$ cells) in the thymus of non-pregnant and E18.5 pregnant $Rank^{WT}$ and $Rank^{\Delta K5}$ females. Data are shown as box-and-whisker plots (from minimal to maximal values); dots represent individual mice. n = 12/7 for $Rank^{WT}$ and n = 7/4 for $Rank^{\Delta K5}$ mice. *P < 0.05; ***P < 0.001. One-way ANOVA, Tukey's post hoc test. **k**, Mean fluorescence intensity (MIF) of CD25, FOXP3, GITR, CTLA-4, neuropilin-1 and Helios in thymic T_{reg} cells of non-pregnant as well as in E13.5–E16.5 pregnant $Rank^{WT}$ and $Rank^{\Delta Foxn1}$ mice. Data are mean ± s.e.m., each dot represents an individual mouse with n = 4–13 animals per group. *P < 0.05; **P < 0.01; ***P < 0.001. One-way ANOVA, Tukey's post hoc test. **l**, Percentage of proliferating ($KI\text{-}67^{+}$) and apoptotic (active $CASP3^{+}$)

$CD4^+FOXP3^+T_{reg}$ cells in the thymus of non-pregnant as well as in E13.5–E16.5 pregnant $Rank^{WT}$ and $Rank^{\Delta Foxn1}$ mice. Data are mean ± s.e.m., each dot represents an individual mouse with $n = 10/5/13/8$ for KI-67 and $n = 6/4/8/7$ for CASP3. $^*P < 0.05$; $^{***}P < 0.001$. One-way ANOVA, Tukey's post hoc test. **m**, Frequencies of T_{reg} cell precursors ($CD25^+FOXP3^-$) and T_{reg} cells ($CD25^+FOXP3^+$) in the thymus of non-pregnant ($n = 10/5$) and E13.5–E16.5 pregnant ($n = 12/7$) $Rank^{WT}$ and $Rank^{\Delta Foxn1}$ females. Data are mean ± s.e.m.; shown as percentage of $CD4^+$ single-positive (SP) thymocytes. Dots represent individual mice. $^*P < 0.05$; $^{***}P < 0.001$. One-way ANOVA, Tukey's post hoc test. **n**, Frequencies of the subsequent mature populations of thymic $CD4^+CD25^+FOXP3^+T_{reg}$ cells, based on CCR7, CCR9, CD69 expression, in the thymus of non-pregnant ($n = 4/4$) and E13.5–E16.5 pregnant ($n = 5/3$) $Rank^{WT}$ and $Rank^{\Delta Foxn1}$ females. Data are mean ± s.e.m., each dot represents an individual mouse. $^*P < 0.05$. One-way ANOVA, Tukey's post hoc test. All data in this figure are from syngeneic C57BL/6J pregnancies.

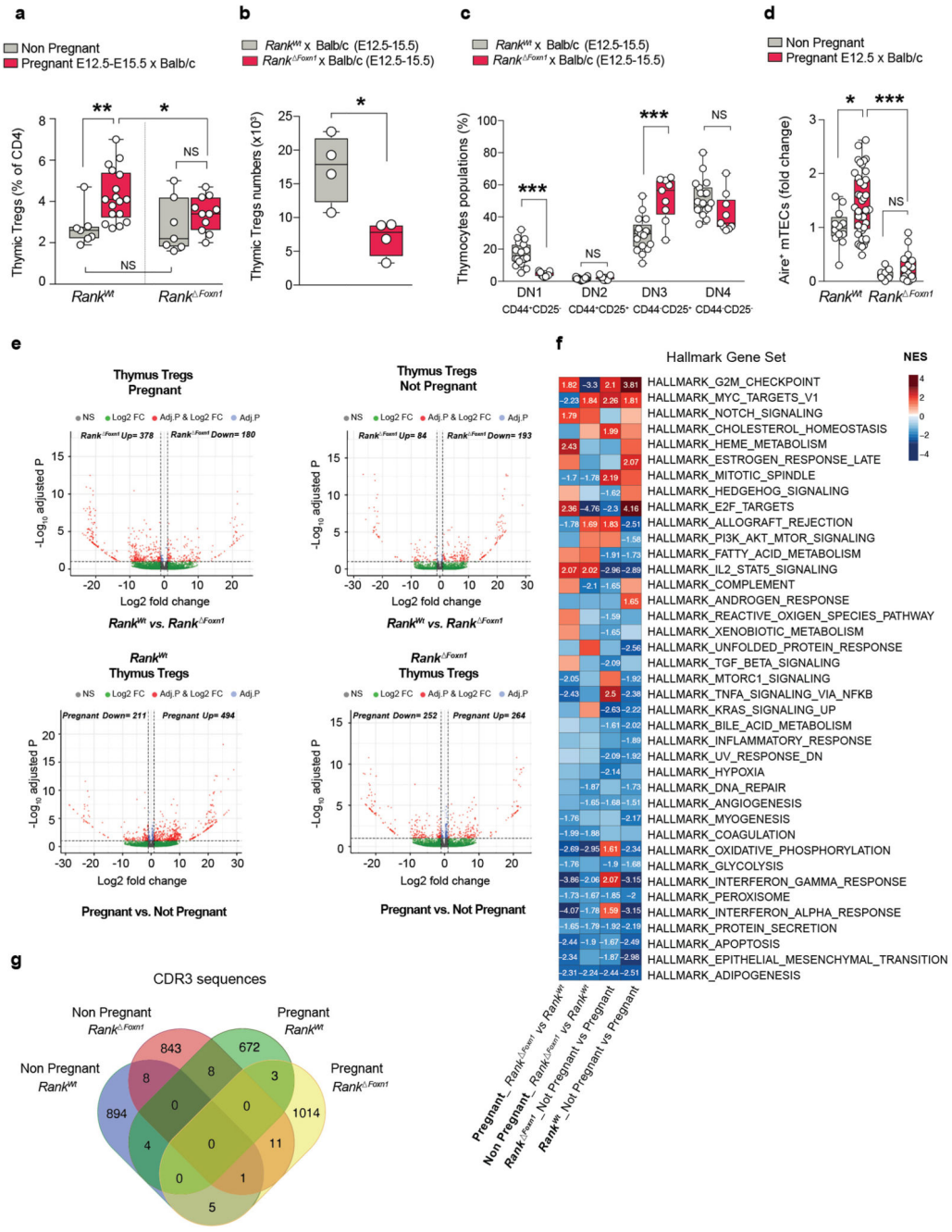

Extended Data Fig. 3. *Rank* $^{\Delta Foxn1}$ thymus in allogeneic pregnancies and transcriptome analysis of thymic T_{reg} cells.

a, Percentages of $CD4^+FOXP3^+T_{reg}$ cells (of total $CD4^+$ cells) in the thymus of individual non-pregnant (n = 7/7) and E12.5–E15.5 pregnant *Rank* ^{WT} and *Rank* $^{\Delta Foxn1}$ females (n = 17/11), crossed to allogeneic BALB/cJ males. *P < 0.05; **P < 0.01. Two-tailed Student's t-test. **b**, Total numbers of $CD4^+FOXP3^+T_{reg}$ cells in the thymus of individual E12.5–E15.5 pregnant *Rank* ^{WT} and *Rank* $^{\Delta Foxn1}$ females (n = 4/4), crossed to allogeneic BALB/cJ males. *P < 0.05. Two-tailed Student's t-test. **c**, Percentages of early developing double negative

Europe PMC Funders Author Manuscripts

(DN) thymocytes (as detected by CD44 and CD25 staining on $CD4^{-}CD8^{-}$ DN populations) in the thymus of E12.5–E15.5 pregnant *Rank* ^{WT} and *Rank* $^{\Delta Foxn1}$ females crossed to allogeneic BALB/cJ males. $n = 18/9$. ***$P < 0.001$. Two-tailed Student's *t*-test. **d**, Relative quantification of $AIRE^{+}$ mTECS in the thymic medullary regions of non-pregnant and E12.5 pregnant *Rank* ^{WT} ($n = 3/7$) and *Rank* $^{\Delta Foxn1}$ ($n = 2/4$) females, crossed to BALB/cJ males, as determined by immunofluorescence (3–6 medullary fields per mouse) and normalized to *Rank* ^{WT} non-pregnant values. *$P < 0.05$. One-way ANOVA, Tukey's post hoc tes). **a**–**d**, The defects and T_{reg} cell deficiencies in *Rank* $^{\Delta Foxn1}$ dams observed in syngeneic pregnancies are also present in allogeneic pregnancies. Data in **a**–**d** are box-and-whisker plots (from minimal to maximal values) and each dot represents an individual data point. **e**, Volcano plots for differentially expressed genes in T_{reg} cells isolated from the thymus of non-pregnant as well as pregnant (E17.5) *Rank* ^{WT} ($n = 4/3$) and *Rank* $^{\Delta Foxn1}$ ($n = 4/4$) female mice. Dots represent genes, colored as: not significant (NS, dark grey); log_2-transformed fold change above threshold (log_2FC; abs(log_2FC) > = 1.0, green); adjusted *P* value above threshold (Adj. P, adjusted $P < = 0.1$, light grey); and significant, with log_2-transformed fold change and adjusted *P* value both above thresholds (red). The numbers of significantly up- and downregulated genes are indicated on each plot. *P* values are based on a two-tailed Wald test and adjusted via the Benjamini–Hochberg procedure. **f**, Summary of GSEA Hallmark gene sets enrichment analysis for the expression profiles of thymic T_{reg} cells isolated from non-pregnant as well as E17.5 pregnant *Rank* ^{WT} ($n = 4/3$) and *Rank* $^{\Delta Foxn1}$ ($n = 4/4$) females. Numbers are normalized enrichment scores (NES) and are only shown for significantly enriched gene set (defined as NES > = 1.4 and FDR < = 10%). **g**, Venn diagram showing the number of unique CDR3 nucleotide sequences identified in the TCRs of thymic T_{reg} cells isolated from non-pregnant as well as E17.5 pregnant *Rank* ^{WT} ($n = 4/3$) and *Rank* $^{\Delta Foxn1}$ ($n = 4/4$) females. Sequences were determined from the RNA-sequencing data using the MiXCR software. For primary data on TCR clones see Supplementary Table 1.

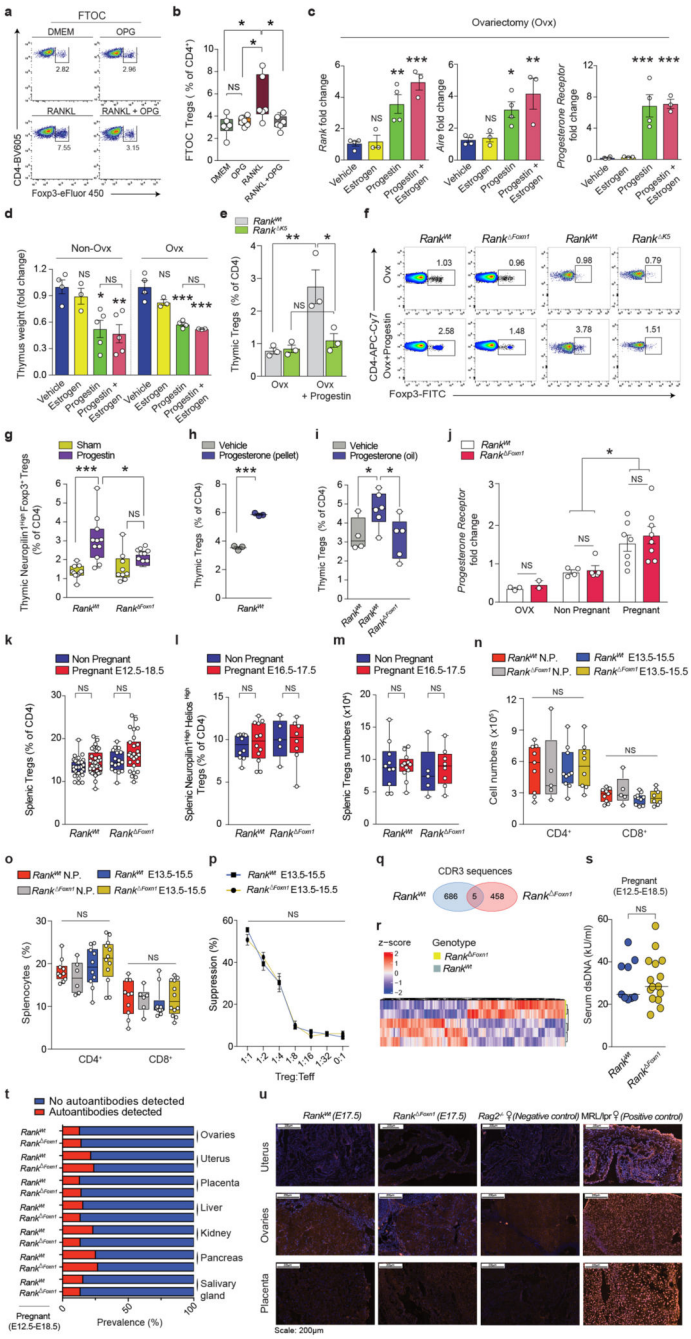

Extended Data Fig. 4. Progesterone-driven thymic T_{reg} cell expansion as well as characterization of splenic T_{reg} cells and autoimmunity in pregnant *Rank* $^{\Delta Foxn1}$ mice.

a, **b**, Representative FACS blots (**a**) and percentages (**b**) of $CD4^+FOXP3^+$ T_{reg} cells (gated on $CD4^+$ cells) in wild-type fetal thymic embryonic lobes (FTOCs) treated with DMEM, RANKL (100 ng ml^{-1}) and/or osteoprotegerin (OPG;1,000 ng ml^{-1}). Data in **b** is a pool of 3 independent experiments, total $n = 6$ per group. Data are shown as box-and-whisker plots (from minimal to maximal values) and each dot represents an individual data point. $^*P <$ 0.05. One-way ANOVA, Tukey's post hoc test. **c**, qPCR analysis for *Rank*, *Aire* and

progesterone receptor (*Pgr*) mRNA expression in the thymus of ovariectomized wild-type C57BL/6J female mice (11 weeks old) that were vehicle-treated ($n = 4$), or subcutaneously-treated with oestrogen (10 μg kg^{-1} daily, $n = 3$), progestin (MPA; 90-day slow-release pellet of 50 mg, $n = 4$), or with both progestin and oestrogen (same doses as single treatments, $n = 3$) for 5 days. Data are mean ± s.e.m., each dot is an individual mouse. $*P < 0.05$; $**P < 0.01$; $***P < 0.001$. One-way ANOVA, Dunnett's post hoc test versus the vehicle group. **d**, Thymus weights in non-ovariectomized (Non-Ovx) and ovariectomized wild-type C57BL/6J female mice (7 weeks and 11 weeks old, respectively) that were vehicle-treated, or subcutaneously-treated with oestrogen, progestin, or with progestin and oestrogen (same hormonal doses as in **c**) for 5 days. Data are mean ± s.e.m., each dot is an individual mouse ($n = 3$–5 per group). $*P < 0.05$; $**P < 0.01$; $***P < 0.001$. One-way ANOVA, Dunnett's post hoc test versus the vehicle group of each cohort. **e**, Percentage of thymic $CD4^+FOXP3^+$ T_{reg} cells (of total $CD4^+$ cells) in $Rank^{WT}$ and $Rank^{\Delta K5}$ ovariectomized females treated with sham surgery or subcutaneously with a progestin-releasing (MPA) pellet for 5 days. Data are mean ± s.e.m., each dot is an individual mouse ($n = 3$). $*P < 0.05$; $**P < 0.01$. One-way ANOVA, Tukey's post hoc test. **f**, Representative FACS blots for thymic T_{reg} cells (gated on single positive $CD4^+$ cells, as shown in Supplementary Data 1) in $Rank^{WT}$ and $Rank^{\Delta Foxn1}$ as well as $Rank^{WT}$ and $Rank^{\Delta K5}$ ovariectomized females treated with sham surgery or subcutaneously with a progestin-releasing (MPA) pellet for 5 days. **g**, Percentages of neuropilin-$1^{high}FOXP3^+$ T_{reg} cells (of total $CD4^+$ cells) in the thymus of sham-treated ($n = 11/9$) and progestin-treated ($n = 11/9$) $Rank^{WT}$ and $Rank^{\Delta Foxn1}$ female mice. Data were determined by FACS analysis. Data are shown as box-and-whisker plots (from minimal to maximal values) and each dot represents an individual mouse. $*P < 0.05$; $***P < 0.001$. One-way ANOVA, Tukey's post hoc test. **h**, Percentages of thymic T_{reg} cells in $Rank^{WT}$ females treated with sham-surgery or treated subcutaneously with progesterone (50 mg/21 day-release pellets) for 6 days ($n = 3$, each dot is an independent mouse and horizontal lines are median, error bars are s.e.m.). $***P < 0.001$. Two-tailed Student's *t*-test. **i**, Percentages of thymic T_{reg} cells in $Rank^{WT}$ mice treated with vehicle (oil, $n = 4$), and $Rank^{WT}$ ($n = 6$) and $Rank^{\Delta Foxn1}$ ($n = 5$) mice treated subcutaneously with progesterone (450 μg in oil per day, $n = 6/5$) for 7 days. Data are shown as box-and-whisker plots (from minimal to maximal values) and each dot represents an individual mouse. $*P < 0.05$. Two-tailed Student's *t*-test. **j**, qPCR analysis for the relative progesterone receptor mRNA expression in the thymus of ovariectomized ($n = 3/2$), non-ovarectomized and non-pregnant ($n = 4/5$), and E12.5–E13.5 pregnant ($n = 7/8$) $Rank^{WT}$ and $Rank^{\Delta Foxn1}$females, which is an expected finding in line with previous studies showing that RANKL/RANK acts downstream of progesterone. Data are mean ± s.e.m. Each dot represents an individual animal. $*P < 0.05$. Two-tailed Student's *t*-test. **k**, Percentages of $CD4^+FOXP3^+$ T_{reg} cells in the spleen of non-pregnant and pregnant (pool from E12.5–E18.5) $Rank^{WT}$ ($n = 29/36$) and $Rank^{\Delta Foxn1}$ ($n = 17/26$) female mice. Two-tailed Student's *t*-test. **l**, Percentages of neuropilin-$1^{high}Helios^{high}$ T_{reg} cells (of total $CD4^+$) in the spleen of non-pregnant and E16.5–E17.5 pregnant $Rank^{WT}$ ($n = 10/12$) and $Rank^{\Delta Foxn1}$ ($n = 5/8$) female mice. Two-tailed Student's *t*-test. **m**, Total numbers of $CD4^+FOXP3^+$ T_{reg} cells in the spleen of non-pregnant and pregnant (pool from E16.5–E17.5) $Rank^{WT}$ ($n = 10/12$) and $Rank^{\Delta Foxn1}$ ($n = 5/8$) female mice. Two-tailed Student's *t*-test. **n**, **o**, Total numbers (**n**) and percentages (**o**) of $CD4^+$ and $CD8^+$ splenocytes in individual non-pregnant ($n = 10/5$) and E13.5–E15.5 pregnant ($n = 12/8$) $Rank^{WT}$ and *Rank*

$^{\Delta Foxn1}$ female mice. One-way ANOVA, Tukey's post hoc test. **k**–**o**, Data are shown as box-and-whisker plots (from minimal to maximal values) and each dot represents an individual mouse. **p**, Percentage of suppression of conventional $CD4^+$T cell proliferation mediated by T_{reg} cells, as determined by flow cytometry using CellTrace Violet dilution, for peripheral (pool of splenic and lymph node) T_{reg} cells isolated from E13.5–E15.5 pregnant *Rank* ^{WT} (n = 5) and *Rank* $^{\Delta Foxn1}$ (n = 3) female mice. Data are mean ± s.e.m. Two-way ANOVA, Sidak's multiple comparisons test. **q**, Venn diagram showing the number of unique CDR3 nucleotide sequences identified in the TCRs of splenic T_{reg} cells isolated from E17.5 pregnant *Rank* ^{WT} (n = 3) and *Rank* $^{\Delta Foxn1}$ (n = 2) females, as identified from the RNA-sequencing data using the MiXCR software. For a summary of clonal distributions see Extended Data Fig. 5g; for primary data on TCR clones see Supplementary Table 1. **r**, Clustered heat map showing the relative expression (z-score) of the 400 top-ranked genes of splenic T_{reg} cells isolated from E17.5 pregnant *Rank* ^{WT} or *Rank* $^{\Delta Foxn1}$ mice. The initial ranking of genes is based on the maximum of the log2-transformed fold change, the absolute value and the statistical significance ranks. Rows indicate genes, columns samples (n = 3/2). **s**, Quantification of serum autoantibodies reactive against double-stranded DNA (dsDNA) in *Rank* ^{WT} (n = 9) and *Rank* $^{\Delta Foxn1}$ (n = 15) pregnant mice (from E12.5–E18.5), determined by ELISA. Values for individual mice (dots) are shown; horizontal lines are median values. Two-tailed Mann–Whitney U-test. **t**, Prevalence (shown as percentages) of *Rank* ^{WT} (n = 7–E14) and *Rank* $^{\Delta Foxn1}$ (n = 8–21) pregnant mice (from E12.5–E18.5) with detectable autoantibodies reactive towards different organs (red bars), as determined by indirect immunofluorescence shown in **k**. No statistically significant differences were observed between the cohorts of *Rank* ^{WT} and *Rank* $^{\Delta Foxn1}$ dams (two-tailed χ^2 test; data not shown). **u**, Images for the detection of autoantibodies (red) by indirect immunofluorescence staining on uterus, ovaries, and placenta sections of *Rag2* $^{-/-}$ mice using serum obtained from pregnant *Rank* ^{WT} and *Rank* $^{\Delta Foxn1}$ mice. Red: autoantibody staining, blue: DAPI. Serum from antibody-deficient *Rag2* $^{-/-}$ as well as autoimmune-prone MRL/lpr females were used as negative and positive controls, respectively. Images are representative of n = 7–14 (*Rank* ^{WT}) and n = 8–21 (*Rank* $^{\Delta Foxn1}$) mice per tissue. All pregnancies in this figure were C57BL/6J syngeneic.

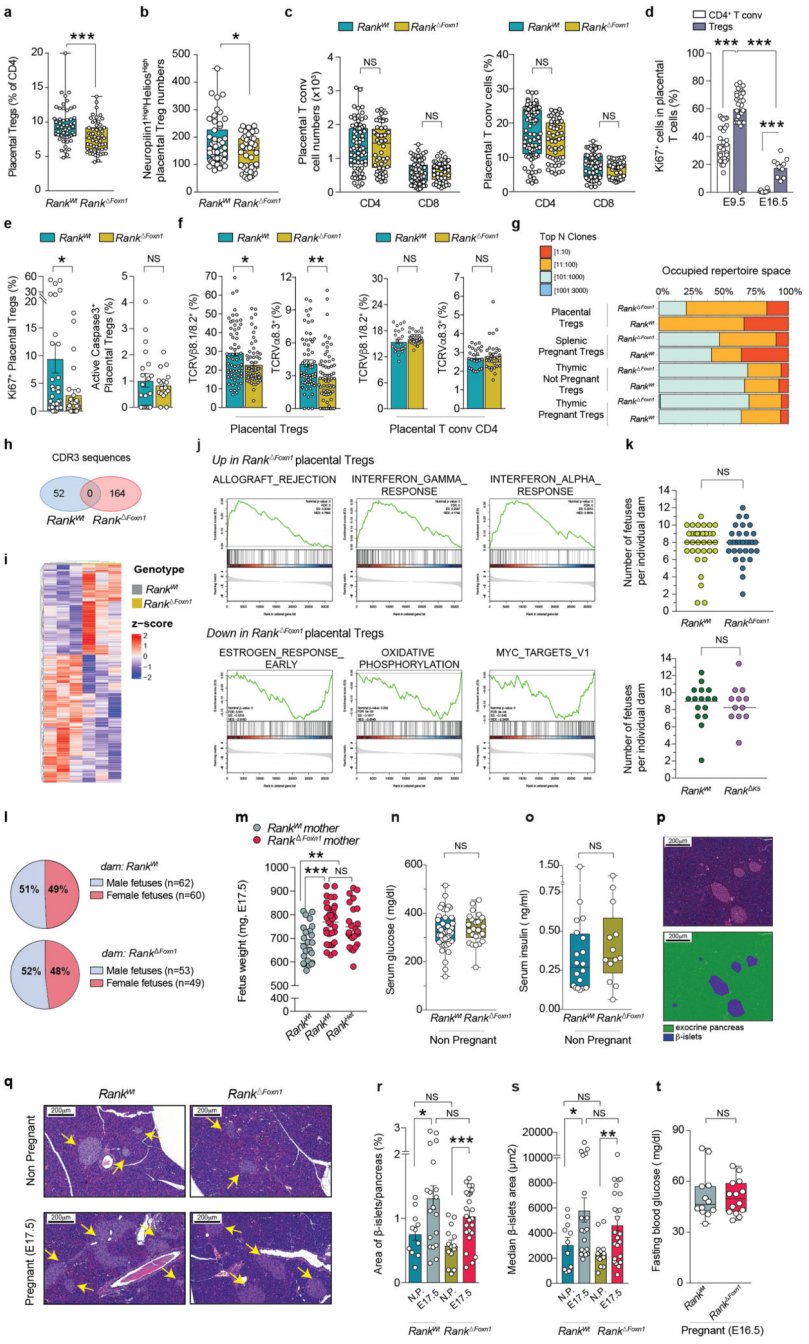

Extended Data Fig. 5. Characterization of the placental T_{reg} cells, fetal macrosomia and glucose metabolism in pregnant *Rank* $^{\Delta Foxn1}$ mice.

a, Percentages of $CD4^+FOXP3^+T_{reg}$ cells (of total $CD4^+$T cells) in E17.5 placentas of *Rank* ^{WT} and *Rank* $^{\Delta Foxn1}$ pregnant mice. Data were determined by FACS and are from individual placentas ($n = 56/54$) isolated from $n = 11/13$ dams, respectively. ***$P < 0.001$. Two-tailed Mann–Whitney *U*-test. **b**, **c**, Total numbers of thymic-derived T_{reg} cells, as determined by neuropilin-$1^{high}Helios^{high}$ expression (**b**), as well as total numbers and percentages of conventional $CD4^+$ and $CD8^+$T cells (**c**) in the E13.5–E16.5 placentas of *Rank* ^{WT} and *Rank*

Europe PMC Funders Author Manuscripts

$^{\Delta Foxn1}$ pregnant mice. n = 39–76 placentas analysed from n = 8–17 dams per group. *P < 0.05. Two-tailed Mann–Whitney U-test. **a**–**c**, Data are shown as box-and-whisker plots (from minimal to maximal values) and each dot represents an individual data point. **d**, Percentage of KI-67^{+}CD4^{+}FOXP3^{+}T$_{reg}$ cells as well as conventional CD4^{+}T cells in the E9.5 and E16.5 placentas of *Rank* ^{WT} mice. Data are mean ± s.e.m., from n = 28/10 individual E9.5 and E16.5 placentas (each dot), respectively. ***P < 0.001. One-way ANOVA, Tukey's post hoc test. **e**, Percentage of KI-67^{+} and active CASP3^{+}T$_{reg}$ cells in the E13.5–E16.5 placentas of *Rank* ^{WT} and *Rank* $^{\Delta Foxn1}$ mice. Data are mean ± s.e.m., from n = 34/27 (for KI-67) and n = 20/17 (Caspase3) individual placentas (each dot) analysed from n = 12/8 (KI-67) and n = 8/7 (Caspase3) *Rank* ^{WT} and *Rank* $^{\Delta Foxn1}$ pregnant females, respectively. *P < 0.05. Two-tailed Mann–Whitney U-test. **f**, Frequency of CD4^{+}FOXP3^{+}T$_{reg}$ cells and conventional CD4^{+}T cells in the E13.5–E17.5 placentas from *Rank* ^{WT} and *Rank* $^{\Delta Foxn1}$ pregnant females expressing TCRVβ8.1/8.2 and TCRVα8.3 receptors, as determined by FACS analysis. The non-significant differences observed in the conventional FOXP3^{-}CD4^{+}T cell population reinforce the thymic origin of the placental T$_{reg}$ cells, as opposed to a peripheral derivation from CD4^{+}T cells. Data are mean ± s.e.m. and are from n = 61–68 (for T$_{reg}$ cells) and n = 36–25 (for conventional CD4^{+}T cells) individual placentas (each dot) analysed from n = 17/17 (for T$_{reg}$ cells) and n = 7/11 (for conventional CD4^{+}T cells) *Rank* ^{WT} and *Rank* $^{\Delta Foxn1}$ pregnant females, respectively. *P < 0.05; **P < 0.01. Two-tailed Mann–Whitney U-test. **g**, Distribution of TCR clonal proportions identified in thymic T$_{reg}$ cells isolated from non-pregnant *Rank* ^{WT} and *Rank* $^{\Delta Foxn1}$ females (n = 4/4), as well as in thymic (n = 3/4), splenic (n = 3/2) and placental (n = 3/3) T$_{reg}$ cells isolated from E17.5 pregnant *Rank* ^{WT} and *Rank* $^{\Delta Foxn1}$ mice. The proportions of the most abundant (top N) TCR clones by the number of next-generation sequencing reads are shown. The increased proportion of reads taken up by the top 1 to 10 (red) and 11 to 110 (orange) clones in placental T$_{reg}$ cells indicates a lower TCR clonal diversity compared to thymus and splenic T$_{reg}$ cells. **h**, Venn diagram showing the number of unique CDR3 nucleotide sequences identified in the TCRs of placental T$_{reg}$ cells isolated from E17.5 pregnant *Rank* ^{WT} (n = 3) and *Rank* $^{\Delta Foxn1}$ (n = 3) females. Data in **g** and **h** was determined from the RNA-sequencing data using the MiXCR software (for primary data on TCR clones see Supplementary Table 1). **i**, Clustered heat map showing the relative expression (z-score) of the 400 top-ranked genes of placental T$_{reg}$ cells isolated from E17.5 pregnant *Rank* ^{WT} and *Rank* $^{\Delta Foxn1}$ mice. The initial ranking of genes is based on the maximum of the log$_2$-transformed fold change, the absolute value and the statistical significance ranks. Rows indicate genes, columns samples (n = 3/3). The genotypes, either *Rank* ^{WT} or *Rank* $^{\Delta Foxn1}$, are annotated for each sample at the top of the columns. **j**, GSEA enrichment plots of the top 3 positively as well as negatively enriched gene sets in the E17.5 placental T$_{reg}$ cells of *Rank* $^{\Delta Foxn1}$ versus *Rank* ^{WT} dams (n = 3 per group). A summary of the GSEA Hallmark gene sets enrichment analysis is shown in Supplementary Table 2. Data from **g**–**j** are from sort-purified neuropilin-1^{high}CD4^{+}FOXP3^{+}T$_{reg}$ cells. **k**, Number of total fetuses (viable + resorbed) gestated per *Rank* ^{WT} (n = 35) and *Rank* $^{\Delta Foxn1}$ (n = 31), as well as *Rank* ^{WT} (n = 16) and *Rank* $^{\Delta K5}$ (n = 12) individual mothers (each dot). Horizontal lines are median values. Two-tailed Mann–Whitney U-test. **l**, Sex distribution of viable fetuses at term (E17.5) born to *Rank* ^{WT} and *Rank* $^{\Delta Foxn1}$ dams. Total numbers and percentage of fetuses per sex are shown for *Rank* ^{WT} (n = 14) and *Rank* $^{\Delta Foxn1}$ (n = 11) dams. No

significant difference was detected in fetal sex distributions between both cohorts (two-tailed χ^2 test; data not shown). Sex was determined by PCR. **m**, Weight of E17.5 fetuses showing that the fetal macrosomia observed in fetuses gestated in *Rank* $^{\Delta Foxn1}$ dams is independent of the *Rank* $^{\Delta Foxn1}$ genotype of the offspring. All pregnancies were syngeneic to C57BL/6J males, thus the offspring of *Rank* $^{\Delta Foxn1}$ dams are either *Rank* ^{WT} wild-type (*Rank* $^{flox/WT}$ *Foxn1* $^{cre-}$) or *Rank* ^{HET} heterozygous (*Rank* $^{flox/WT}$ *Foxn1* $^{cre+}$) for RANK expression in the thymus; both groups are macrosomic compared to *Rank* ^{WT} (*Rank* $^{flox/flox}$ *Foxn1* $^{cre-}$) fetuses from *Rank* ^{WT} dams. Each dot represents an individual fetus, with $n = 7–54$ mice per group. Horizontal lines are mean, error bars are s.e.m. $^{**}P < 0.01$; $^{***}P < 0.001$. Two-tailed Student's *t*-test. **n**, **o**, Serum glucose (**n**; $n = 42/26$) and insulin (**o**; $n = 20/13$) levels in ad libitum-fed individual non-pregnant *Rank* ^{WT} and *Rank* $^{\Delta Foxn1}$ females. These are the littermate controls of the pregnant cohorts shown in Fig. 2e, f. **n**, **o**, Data are shown as box-and-whisker plots (from minimal to maximal values) and each dot represents an individual mouse. Two-tailed Student's *t*-test (n) and two-tailed Mann–Whitney *U*-test (o). **p**, Images for the quantification of β-islet areas using the Definiens Tissue software to identify and categorize β-islets (blue) and the exocrine pancreas (green). Representative of $n > 120$ slides analysed. **q**, H&E-stained pancreas cross-sections for non–pregnant (upper panels) and E17.5 pregnant (lower panels) *Rank* ^{WT} and *Rank* $^{\Delta Foxn1}$ mice, depicting the expected enlargement of insulin-producing β-islets (arrows) during pregnancy, in both *Rank* ^{WT} and *Rank* $^{\Delta Foxn1}$ dams. Representative of $n = 11–25$ slides analysed per group. **r**, **s**, Relative total area of pancreatic β-islets (**r**) and median β-islets area (**s**) in non-pregnant and E17.5 pregnant *Rank* ^{WT} ($n = 5/9$) and *Rank* $^{\Delta Foxn1}$ ($n = 7/13$) mice, determined as shown in **p** (2 distal sections per mouse). $^{*}P < 0.05$; $^{**}P < 0.01$; $^{***}P < 0.001$. Two-tailed Student's *t*-test. Data are mean ± s.e.m., each dot represents an individual data point. **t**, Fasting blood glucose levels in E16.5 pregnant *Rank* ^{WT} and *Rank* $^{\Delta Foxn1}$ mice. Data are shown as box-and-whisker plots (from minimal to maximal values) and each dot represents an individual dam, $n = 12/14$. Two-tailed Student's *t*-test. All pregnancies in this figure were from C57BL/6J syngeneic crosses.

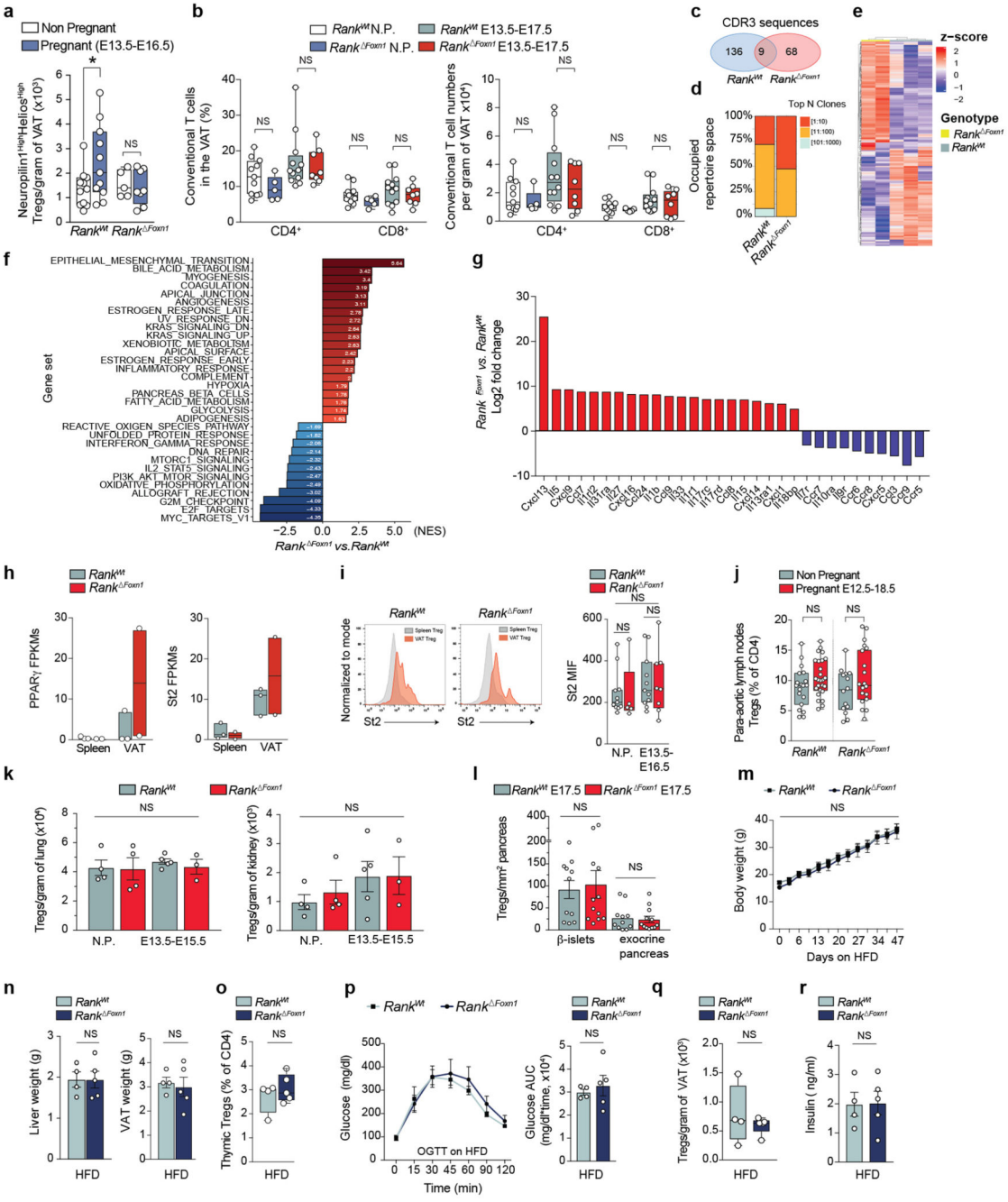

Extended Data Fig. 6. Characterization of T_{reg} cells in the VAT and other tissues in pregnant *Rank* $^{\Delta Foxn1}$ mice.

a, Total numbers of neuropilin-1^{high}Helios^{high}CD4^{+}FOXP3^{+} cells T_{reg} cells (indicative of thymic origin), per gram of visceral white adipose tissue (gonadal VAT) in non-pregnant (n = 11/5) and E13.5–E16.5 pregnant (n = 11/8) *Rank* ^{WT} and *Rank* $^{\Delta Foxn1}$ females. Data are shown as box-and-whisker plots (from minimal to maximal values) and each dot represents an individual mouse. Data were determined by FACS analysis. *P < 0.05. Two-tailed Student's t-test. **b**, Percentages and total numbers of conventional CD4^{+} and CD8^{+}T cells

Europe PMC Funders Author Manuscripts

per gram of visceral white adipose tissue (gonadal VAT) in non-pregnant (n = 11/5) and E13.5–E17.5 pregnant (n = 12/8) *Rank* ^{WT} and *Rank* $^{\Delta Foxn1}$ females. Data are shown as box-and-whisker plots (from minimal to maximal values) and each dot represents an individual mouse. Data were determined by FACS analysis. Two-tailed Mann–Whitney U-test. **c**, Venn diagram showing the number of unique CDR3 nucleotide sequences identified in the TCRs of VAT (gonadal) T_{reg} cells isolated from E17.5 pregnant *Rank* ^{WT} (n = 3) and *Rank* $^{\Delta Foxn1}$ (n = 2) females. **d**, Distribution of TCR clonal proportions identified in VAT T_{reg} cells isolated from E17.5 pregnant *Rank* ^{WT} (n = 3) and *Rank* $^{\Delta Foxn1}$ (n = 2) mice. The proportions of the most abundant (top N) TCR clones by the number of next-generation sequencing reads are shown. Data from **c** and **d** were determined using the MiXCR software (for primary data on TCR clones see Supplementary Table 1). **e**, Clustered heat maps showing the relative expression (z-score) of the 400 top-ranked genes of VAT T_{reg} cells isolated from E17.5 pregnant *Rank* ^{WT} or *Rank* $^{\Delta Foxn1}$ mice. The initial ranking of genes is based on the maximum of the $\log_2$-transformed fold change, the absolute value and the statistical significance ranks. Rows indicate genes, columns samples. The genotypes, either *Rank* ^{WT} (n = 3) or *Rank* $^{\Delta Foxn1}$ (n = 2), are annotated for each sample at the top of the columns. **f**, Summary of GSEA Hallmark gene sets enrichment analysis for the expression profiles of VAT T_{reg} cells isolated from E17.5 pregnant *Rank* $^{\Delta Foxn1}$ (n = 2) versus *Rank* ^{WT} (n = 3) females. Numbers are NES and all gene sets shown are significantly enriched (defined as NES > = 1.4 and false discovery rate FDR < = 10%). Red, positively enriched gene sets in *Rank* $^{\Delta Foxn1}$; blue, positively enriched gene sets in *Rank* ^{WT} (the full list of gene sets is shown in Supplementary Table 3). **g**, Bar plot showing $\log_2$-transformed fold change of expression for cytokines and chemokines genes in VAT T_{reg} cells isolated from E17.5 pregnant *Rank* $^{\Delta Foxn1}$ (n = 2) versus *Rank* ^{WT} (n = 3) mice, as determined by RNA sequencing. Red and blue denote significantly up- and downregulated genes in *Rank* $^{\Delta Foxn1}$, respectively (defined as abs($\log_2$FC) > = 1.0 and adjusted P < = 0.1). **h**, Expression levels (in Fragments per Kilobase Million -FPKM) of the signature VAT T_{reg} cells markers PPARγ and ST2 (IL-33R) in splenic and VAT T_{reg} cells from E17.5 pregnant *Rank* ^{WT} (n = 3) and *Rank* $^{\Delta Foxn1}$ females (n = 2); as determined by RNA sequencing. Floating bars run from minimal to maximal values; lines are median and dots are individual mouse. **i**, Left, Representatives FACS histograms for ST2 expression in T_{reg} cells from the spleen and gonadal VAT of E13.5–E16.5 *Rank* ^{WT} and *Rank* $^{\Delta Foxn1}$ pregnant mice. Right, Mean fluorescence intensity (MIF) of ST2 in T_{reg} cells from gonadal VAT of non-pregnant as well as E13.5–E16.5 *Rank* ^{WT} (n = 11/11) and *Rank* $^{\Delta Foxn1}$ (n = 5/8) pregnant mice. Data were determined by FACS and are shown as box-and-whisker plots (from minimal to maximal values) with each dot representing an individual mouse. Kruskal–Wallis test, Dunn's post-test. **j**, Percentages of $CD4^+FOXP3^+T_{reg}$ cells (of total $CD4^+$ cells) in the uterus-draining para-aortic lymph nodes of individual non-pregnant and pregnant (pool from E12.5–E18.5) *Rank* ^{WT} (n = 19/26) and *Rank* $^{\Delta Foxn1}$ (n = 14/19) female mice, as determined by FACS. Data are shown as box-and-whisker plots (from minimal to maximal values) and each dot represents an individual mouse. Two-tailed Student's t-test. **k**, Numbers of $CD4^+FOXP3^+T_{reg}$ cells per gram of lung and kidney of individual non-pregnant (n = 5/5) and E13.5–E15.5 pregnant (n = 5/3) *Rank* ^{WT} and *Rank* $^{\Delta Foxn1}$ female mice, as determined by FACS. Data are mean ± s.e.m., each dot represents an individual mouse. One-way ANOVA, Tukey's post hoc test. **l**, Numbers of $CD4^+FOXP3^+T_{reg}$ cells per mm^2 in β-islets

and exocrine pancreas of E17.5 pregnant *Rank* ^{WT} (n = 11) and *Rank* $^{\Delta Foxn1}$ (n = 13) mice, as determined by immunohistochemistry. Data are mean ± s.e.m., each dot represents an individual mouse. Two-tailed Mann–Whitney *U*-test. **m**, Body weight increases for *Rank* ^{WT} or *Rank* $^{\Delta Foxn1}$ female mice (n = 4/5) fed a HFD for 47 days. Data are mean ± s.e.m. Two-way ANOVA, Sidak's multiple comparison test. **n**, Liver and visceral white adipose tissue (gonadal VAT) weights in *Rank* ^{WT} and *Rank* $^{\Delta Foxn1}$ female mice (n = 4/5) fed a HFD for 7 weeks. Data are mean ± s.e.m., each dot represents an individual mouse. Two-tailed Student's *t*-test. **o**, Percentages of $CD4^+FOXP3^+T_{reg}$ cells in the thymus of *Rank* ^{WT} (n = 4) and *Rank* $^{\Delta Foxn1}$ (n = 5) females fed a HFD for 7 weeks, as determined by FACS. Data are shown as box-and-whisker plots (from minimal to maximal values) and each dot represents an individual mouse. Two-tailed Mann–Whitney *U*-test. **p**, Oral glucose-tolerance test (mean ± s.e.m.) and the corresponding area under the curve (AUC) calculations (data are mean ± s.e.m., values for individual mice are shown) for *Rank* ^{WT} and *Rank* $^{\Delta Foxn1}$ females fed a HFD for 7 weeks (n = 4/5). Two-tailed Student's *t*-test. **q**, Total numbers of $CD4^+FOXP3^+T_{reg}$ cells per gram of VAT in *Rank* ^{WT} and *Rank* $^{\Delta Foxn1}$ females fed a HFD for 7 weeks. Data are shown as box-and-whisker plots (from minimal to maximal values) and each dot represents an individual mouse (n = 4/5). Data were determined by FACS analysis. Two-tailed Mann–Whitney *U*-test. **r**, Serum levels of insulin in *Rank* ^{WT} and *Rank* $^{\Delta Foxn1}$ females fed ad libitum a HFD for 7 weeks (n = 4/5). Data are mean ± s.e.m., each dot represents an individual mouse. Two-tailed Student's *t*-test.

Europe PMC Funders Author Manuscripts

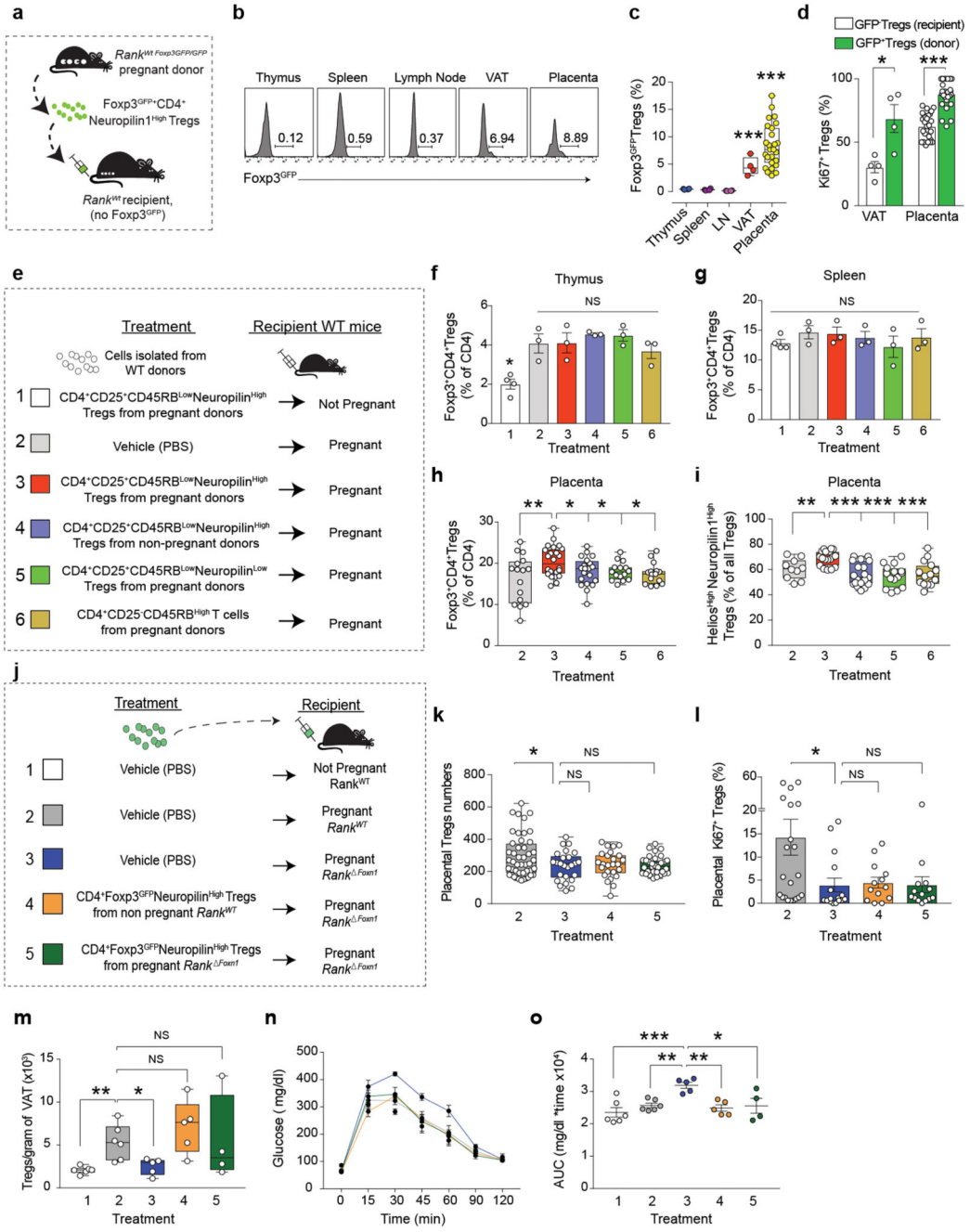

Extended Data Fig. 7. T_{reg} cell transplantation studies.

a, T_{reg}-cell adoptive-transfer experimental design to assess the migration of the transplanted pregnancy-associated T_{reg} cells into different organs. Recipient early pregnant (E3.5–E5.5) *Rank* ^{WT} females (no *Foxp3* ^{GFP} transgene) were inoculated (intravenous inoculation) with 3 × 10^5 sort-purified FOXP3–GFP$^+$CD4$^+$neuropilin-1^{high} T_{reg} cells isolated from E6.5–E8.5 *Rank* ^{WT} *Foxp3* $^{GFP/GFP}$ pregnant donors. **b**, **c**, Representative histograms (**b**) and relative percentage (**c**) of FOXP3–GPF$^+$ transplanted T_{reg} cells (of total T_{reg} cells) in the thymus, spleen, draining (peri-uterine) lymph nodes, gonadal VAT and placentas of recipient *Rank*

Rank ^{WT} wild-type pregnant females 5 days after transfer, as described in **a**. $n = 4$ recipient mice and $n = 26$ placentas were analysed. Data are shown as box-and-whisker plots (from minimal to maximal values) and each dot represents an individual data point. $^{***}P < 0.001$ versus thymus, spleen or draining lymph nodes. One-way ANOVA, Dunnett's post hoc test. **d**, Percentage of KI-67^{+}GFP^{-}(recipients') and KI-67^{+}GFP^{+} (donors') T_{reg} cells in the gonadal VAT and placentas of recipient *Rank* ^{WT} wild-type pregnant females 5 days after transfer, as described in **a**. Data are mean ± s.e.m., each dot represents an individual data point from $n = 4$ (for VAT) and $n = 26$ (for placenta). $^{*}P < 0.05$; $^{***}P < 0.001$. Two-tailed Mann–Whitney *U*-test. **e**, Schematics of the adoptive T_{reg} cell transfer study used to determine which cell type migrates to the placenta (only wild-type animals were used). Since mice did not express the *Foxp3* ^{GFP} transgene, T_{reg} cells were sorted as CD4^{+}CD25^{+}CD45RB^{low} cells and conventional T CD4 cells as CD4^{+}CD25^{-}CD45RB^{high}. T_{reg} cells of thymic origin (neuropilin-1^{high}) were transplanted from pregnant donors into non-pregnant females (1). Vehicle-treated control pregnant recipients received only PBS (2). neuropilin-1^{high} T_{reg} cells isolated from pregnant (3) or non-pregnant donors (4) were transplanted into pregnant recipients. Finally, neuropilin-1^{low} T_{reg} cells (5) as well as conventional CD4^{+}CD25^{-}CD45RB^{high} T cells (6) were transferred from pregnant donors to recipient dams. In all cases, cells were sorted and pooled from spleen, lymph nodes and thymus of donors and transferred (intravenous inoculation, 1×10^{5}) into early (E0.5–E2.5) pregnant mice. All recipients were euthanized 15 days post transfer (E15.5–E17.5) for FACS analysis of T_{reg} cells in thymus, spleen and placentas shown in **f**–**i**. **f**, **g**, Percentages of CD4^{+}FOXP3^{+}T_{reg} cells (of total CD4^{+}) in the thymus (**f**) and spleen (**g**) of recipient mice treated with different T cells as described in **e**, at the experimental end point ($n = 4$–3 mice per group). Data are mean ± s.e.m., each dot represents an individual mouse. $^{*}P < 0.05$. Two-tailed Student's *t*-test. **h**, Percentages of CD4^{+}FOXP3^{+}T_{reg} cells (of CD4^{+}), as well as **i**, neuropilin-1^{high}Helios^{high} T_{reg} cells (of all CD4^{+}FOXP3^{+}T_{reg} cells) in the E15.5–E17.5 placentas of recipient mice treated as described in **e**. Data are shown as box-and-whisker plots (from minimal to maximal values) and each dot represents an individual placenta. $n =$ 10–24 individual placentas from $n = 3$ recipient mice were analysed per group. $^{*}P < 0.05$; $^{**}P < 0.01$. Two-tailed Student's *t*-test versus group 3. **j**, T_{reg}-cell adoptive-transfer scheme to assess whether T_{reg} cells from non-pregnant *Rank* ^{WT} or from pregnant *Rank* $^{\Delta Foxn1}$ females can rescue placental T_{reg} cell numbers and altered glucose metabolism in *Rank* $^{\Delta Foxn1}$ dams. As in the transplant study shown in Fig. 3a, thymic T_{reg} cells were sorted and pooled from spleen, thymus and lymph nodes defined as CD4^{+}FOXP3–GFP $^{+}$neuropilin-1^{high} T_{reg} cells (thymic T_{reg} cells). Both donor (E9.5) and recipient mice contained the FOXP3^{GFP} transgene and 1×10^{5} T_{reg} cells were transplanted at E.0.5–E2.5. Vehicle was PBS. **k**, **l**, Total numbers of T_{reg} cells (**k**) and percentages of KI-67^{+}T_{reg} cells (**l**) in the E16.5 placentas of vehicle-treated *Rank* ^{WT} (2) and *Rank* $^{\Delta Foxn1}$ (3) pregnant mice, as well as E16.5 placentas of *Rank* $^{\Delta Foxn1}$ pregnant mice treated with thymic T_{reg} cells isolated from non-pregnant *Rank* ^{WT} females (4) or isolated from pregnant *Rank* $^{\Delta Foxn1}$ females (5) as described in **j**. Data were obtained by FACS analysis and are shown as box-and-whisker plots (**k**, from minimal to maximal values) and bar charts (**l**, mean ± s.e.m.) from $n =$ 46/25/25/32 for **k**, and $n = 21/16/13/14$ for **l**, individual placentas (each dot) analysed from n = 6/5/5/4 mice for groups 2 to 5 respectively. $^{*}P < 0.05$. One-Way ANOVA, Dunnett's multiple comparison test versus group 3. **m**, Total numbers of CD4^{+}FOXP3^{+}T_{reg} cells per

gram of gonadal VAT in vehicle-treated non-pregnant *Rank* ^{WT} females (group 1), vehicle-treated *Rank* ^{WT} (2) and *Rank* $^{\Delta Foxn1}$ (3) E16.5 pregnant mice, as well as *Rank* $^{\Delta Foxn1}$ E16.5 pregnant mice treated with thymic T_{reg} cells isolated from non-pregnant *Rank* ^{WT} females (4) or from pregnant *Rank* $^{\Delta Foxn1}$ females (5) as described in **j**. Data were obtained by FACS analysis and are from n = 6/6/5/5/4 mice for groups 1 to 5, respectively. Data are shown as box-and-whisker plots (from minimal to maximal values) and each dot represents an individual mouse. *P < 0.05; **P < 0.01. Two-tailed Student's t-test versus group 2. **n**, **o**, Oral glucose-tolerant test (**n**; mean ± s.e.m.) and the corresponding area under the curve calculations (**o**) in vehicle-treated non-pregnant *Rank* ^{WT} females (group 1), vehicle-treated *Rank* ^{WT} (2) and *Rank* $^{\Delta Foxn1}$ (3) E15.5 pregnant mice, as well as *Rank* $^{\Delta Foxn1}$ E15.5 pregnant females treated with thymic T_{reg} cells isolated from non-pregnant *Rank* ^{WT} females (4) or from pregnant *Rank* $^{\Delta Foxn1}$ females (5) as described in **j**. n = 6/6/5/5/4 mice for groups 1–5, respectively. Lines in scatter dot plots are mean, error bars are s.e.m. *P < 0.05; **P < 0.01; ***P < 0.001. One-way ANOVA, Dunnett's multiple comparisons test versus group 3.

Europe PMC Funders Author Manuscripts

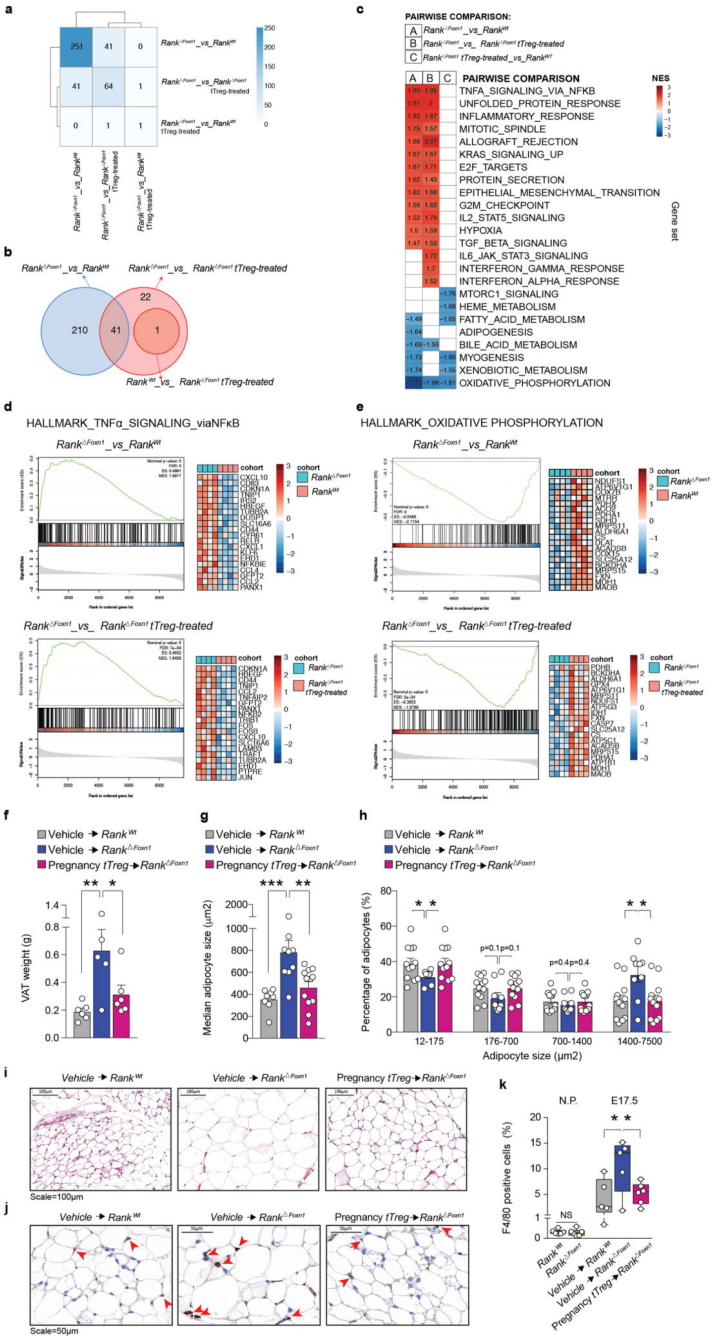

Extended Data Fig. 8. Gene expression profiling and characterization of the VAT in pregnant *Rank* $^{\Delta Foxn1}$ mice.

a, **b**, Pairwise intersection heat map showing the numbers of differentially expressed genes in the gonadal VAT (**a**) as well as overlap counts (**b**) resulting from all pairwise comparisons of the three experimental conditions: vehicle-treated E17.5 pregnant *Rank* ^{WT}, as well as E17.5 *Rank* $^{\Delta Foxn1}$ pregnant females treated with either vehicle- or with sort-purified FOXP3–GFP^{+}CD4^{+}neuropilin-1^{high} T_{reg} cells isolated from *Rank* ^{WT} *Foxp3* $^{GFP/GFP}$ pregnant donors (pregnancy tT_{reg}-cell-treated). DESeq2 v.1.16.1, FDR threshold of 0.05. **c**,

Summary of GSEA Hallmark gene sets significantly enriched (NES > = 1.4 and FDR < = 10%) comparing the expression profiles (in CPM) of the visceral (gonadal) white adipose tissue of *Rank* $^{\Delta Foxn1}$, *Rank* ^{WT}, and *Rank* $^{\Delta Foxn1}$ tT_{reg}-cell-treated dams at E17.5 (n = 4 per group). NES scores are only listed for the significant sets. **d**, **e**, GSEA enrichment plots of the top positively enriched gene set: (TNF signalling via NF-κB), as well as the top negatively enriched gene set (oxidative phosphorylation) in the VAT of *Rank* $^{\Delta Foxn1}$ versus *Rank* ^{WT} as well as *Rank* $^{\Delta Foxn1}$ versus *Rank* $^{\Delta Foxn1}$ dams at E17.5 treated with thymic T_{reg} cells (n = 4 per group). GSEA-derived heat maps on the right show the relative level of gene expression (red, high; blue, low) in the leading edge subset (top 20 genes shown). All mice described in this figure were treated as described in Fig. 3a. *Rank* $^{\Delta Foxn1}$ versus *Rank* ^{WT} dams were treated with vehicle (PBS), which for simplification is not shown in the figure. **f**, Total adipose tissue weights and **g**, median adipocyte sizes in the gonadal VAT of vehicle-treated E17.5 pregnant *Rank* ^{WT} mice (n = 6) as well as *Rank* $^{\Delta Foxn1}$ recipient E17.5 pregnant females treated with either vehicle (n = 5) or with sort-purified FOXP3–GFP $^{+}$CD4^{+}neuropilin-1^{high} T_{reg} cells isolated from *Rank* ^{WT} *Foxp3* $^{GFP/GFP}$ pregnant donors (n = 6; that is, pregnancy tT_{reg}-cell-treated). T_{reg}-cell adoptive transfer was performed as shown in Fig. 3a. Data are mean ± s.e.m., each dot represents an individual data point. *P < 0.05; **P < 0.01; ***P < 0.001. One-way ANOVA, Dunnett's post hoc test. **h**, Percentages of different adipocytes sizes in the VAT of vehicle-treated *Rank* ^{WT} dams (n = 6) as well as vehicle- and pregnancy tT_{reg}-cell-treated *Rank* $^{\Delta Foxn1}$ dams at E17.5 (n = 5 and 6, respectively). *P < 0.05; other P values are shown. Two-tailed Student's t-test. For **g** and **h**, two distal cross-sections were analysed per mouse. Data are mean ± s.e.m., each dot represents an individual data point. **i**, H&E cross-sections of the gonadal white adipose tissue of vehicle-treated *Rank* ^{WT} dams, as well as vehicle- and pregnancy tT_{reg}-cell-treated *Rank* $^{\Delta Foxn1}$ dams at E17.5, showing markedly enlarged adipocytes in *Rank* $^{\Delta Foxn1}$ pregnant mice compared with *Rank* ^{WT} and pregnancy tT_{reg}-cell-treated *Rank* $^{\Delta Foxn1}$ counterparts. Representative of n = 10–12 slides analysed from 5–6 mice per group. **j**, Immunohistochemistry detecting F4/80^{+} macrophages (arrows) in the VAT of vehicle-treated *Rank* ^{WT}, as well as of vehicle- and pregnancy tT_{reg}-cell-treated *Rank* $^{\Delta Foxn1}$ dams at E17.5. Representative of n = 5–6 mice analysed. **k**, Percentages of F4/80^{+} macrophages in the VAT of non-pregnant *Rank* ^{WT} and *Rank* $^{\Delta Foxn1}$ females as well as vehicle-treated *Rank* ^{WT} and vehicle- and pregnancy tT_{reg}-cell-treated *Rank* $^{\Delta Foxn1}$ dams at E17.5, as detected by immunohistochemistry and quantified using the Definiens Software (n = 5–6 per genotype). Data are shown as box-and-whisker plots (from minimal to maximal values) and each dot represents an individual mouse. *P < 0.05. One-way ANOVA, Tukey's post hoc test.

Europe PMC Funders Author Manuscripts

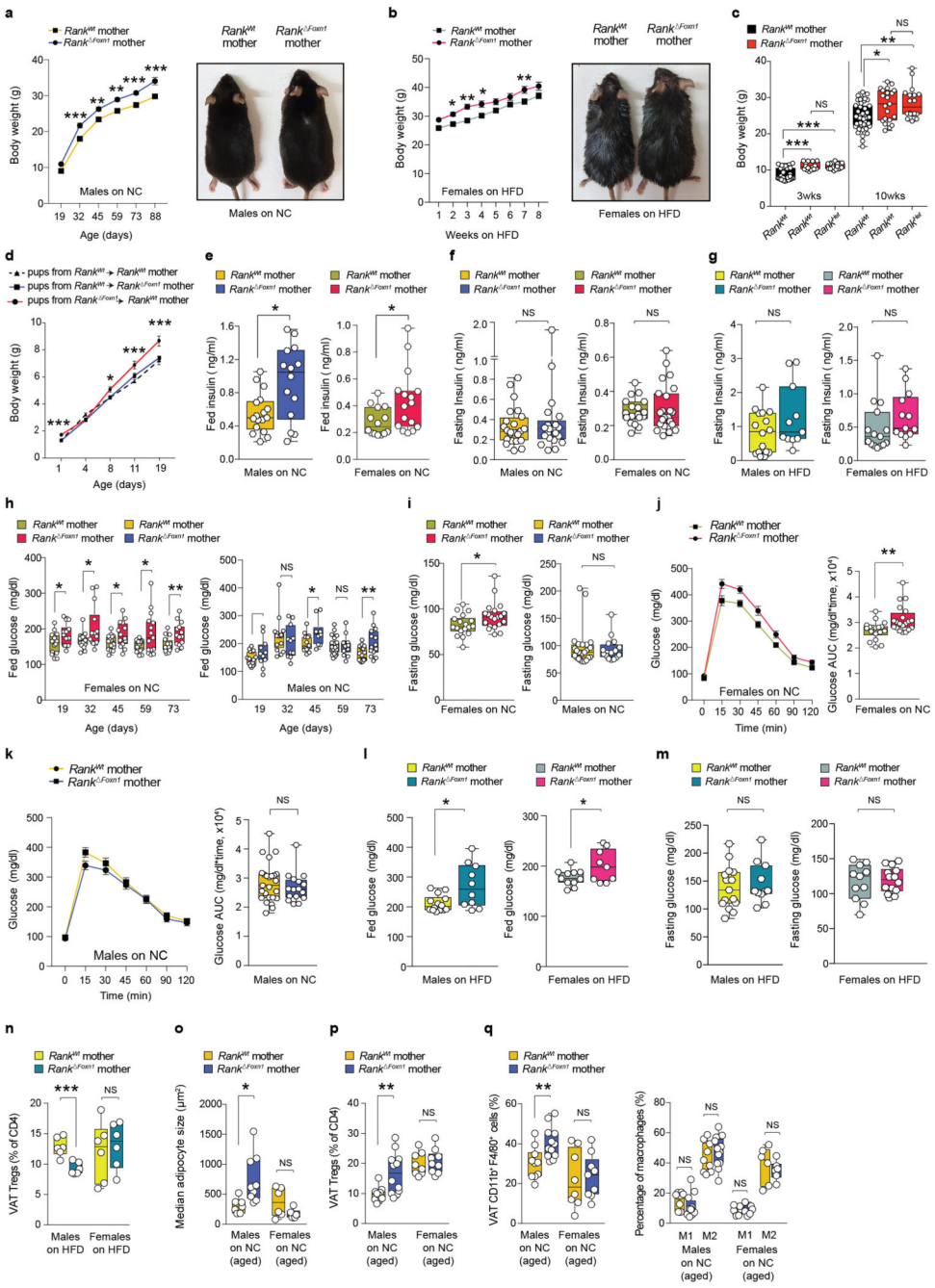

Extended Data Fig. 9. Macrosomia, VAT and glucose metabolism in the offspring of *Rank* $^{\Delta Foxn1}$ dams.

a, Body weights (mean ± s.e.m.) and representative photograph (at 80 days of age) for the male offspring of *Rank* ^{WT} or *Rank* $^{\Delta Foxn1}$ dams (n = 16/11) fed a normal chow (NC). Data from female offspring are shown in Fig. 4a. $^{**}P < 0.01$; $^{***}P < 0.001$. Two-way ANOVA, Sidak's multiple comparison test. **b**, Body weights (mean ± s.e.m.) and representative photograph (taken after 6 weeks on a HFD) for the female offspring of *Rank* ^{WT} or *Rank* $^{\Delta Foxn1}$ dams (n = 14/12) fed a HFD. Male comparisons are shown in Fig. 4b. $^{*}P < 0.05$; $^{**}P$

< 0.01. Two-way ANOVA, Sidak's multiple comparison test. **c**, Body weights at 3 and 10 weeks of age for the different genotypes of the offspring of *Rank* $^{\Delta Foxn1}$ dams as compared to those from *Rank* ^{WT} dams. All pregnancies were syngeneic to C57BL/6J males, thus the offspring of *Rank* $^{\Delta Foxn1}$ dams are either *Rank* ^{WT} wild-type (*Rank* $^{flox/WT}$ *Foxn1* $^{cre-}$) or *Rank* ^{HET} heterozygous (*Rank* $^{flox/WT}$ *Foxn1* $^{cre+}$) for RANK expression in the thymus; both groups are macrosomic compared to *Rank* ^{WT} (*Rank* $^{flox/flox}$ *Foxn1* $^{Cre-}$) fetuses from *Rank* ^{WT} dams. Offspring of different genotypes were co-caged to minimize microbiota effects. Data are shown as box-and-whisker plots (from minimal to maximal values); dots represent individual mice, with n = 16–45 per group. *P < 0.05; **P < 0.01; ***P < 0.001. Kruskal–Wallis test, Dunn's post-test. **d**, Body weights from postnatal day 1 until weaning (day 19) for pups born to *Rank* $^{\Delta Foxn1}$ dams but caged and breast-fed by *Rank* ^{WT} dams (n = 18), as well as the pups born to *Rank* ^{WT} dams but caged and breast-fed by *Rank* $^{\Delta Foxn1}$ dams (n = 21). As controls, pups born and breast-fed to *Rank* ^{WT} dams are shown (n = 11). Mothers were exchanged at day 1 after birth. Note the macrosomia is inherent to the pups and does not depend on mothers or breast milk-derived effects. Data are mean ± s.e.m. *P < 0.05; **P < 0.01; ***P < 0.001. Two-way ANOVA, Dunnett's multiple comparison test. **e**, **f**, Ad libitum-fed (**e**) and fasting (**f**) serum insulin levels in male and female offspring of *Rank* ^{WT} and *Rank* $^{\Delta Foxn1}$ dams fed a normal chow (NC) diet for 80 days. Data are shown as box-and-whisker plots (from minimal to maximal values). Dots represent individual mice, with n = 14–24 per group. *P < 0.05. Two-tailed Mann–Whitney U-test. **g**, Fasting serum insulin levels in male (n = 16/11) and female (n = 15/13) offspring of *Rank* ^{WT} and *Rank* $^{\Delta Foxn1}$ dams fed a HFD for 9 weeks. Data are shown as box-and-whisker plots (from minimal to maximal values) and each dot represents an individual mouse. Two-tailed Mann–Whitney U-test. **h**, Ad libitum-fed blood glucose levels at different ages of females (n = 14–25) and males (n = 10–23) offspring of *Rank* ^{WT} or *Rank* $^{\Delta Foxn1}$ dams fed a normal chow (NC). Data are shown as box-and-whisker plots (from minimal to maximal values) and each dot represents an individual mouse. *P < 0.05; **P < 0.01. Two-tailed Student's t-test. **i**, Fasting blood glucose levels in female (n = 18/20) and male (n = 25/16) offspring of *Rank* ^{WT} or *Rank* $^{\Delta Foxn1}$ dams that were fed a normal chow for 80 days. Data are shown as box-and-whisker plots (from minimal to maximal values) and each dot represents an individual mouse. *P < 0.05. Two-tailed Mann–Whitney U-test. **j**, **k**, Oral glucose-tolerance test (mean ± s.e.m.) and the corresponding area under the curve calculations for the female (**j**, n = 18/20) and male offspring (**k**, n = 25/16) of *Rank* ^{WT} and *Rank* $^{\Delta Foxn1}$ dams. Data are shown as box-and-whisker plots (from minimal to maximal values) and each dot represents an individual mouse, fed 80 days a normal chow diet. **P < 0.01. Two-tailed Mann–Whitney U-test. **l**, **m**, Ad libitum-fed (**l**) and fasting (**m**) blood glucose levels in male and female offspring of *Rank* ^{WT} and *Rank* $^{\Delta Foxn1}$ dams fed a HFD for 9 weeks. Data are shown as box-and-whisker plots (from minimal to maximal values) and each dot represents an individual mouse. n = 9–15. *P < 0.05. Two-tailed Student's t-test. **n**, Percentages of $CD4^+FOXP3^+$ VAT T_{reg} cells (of total CD4) in the gonadal white adipose tissue of the HFD-fed male and female offspring of *Rank* ^{WT} (n = 6/6) and *Rank* $^{\Delta Foxn1}$ (n = 6/6) dams. Mice were fed a HFD for 12 weeks. Data are shown as box-and-whisker plots (from minimal to maximal values) and each dot represents an individual mouse. ***P < 0.001. Two-tailed Student's t-test. **o**, Median adipocyte sizes in the gonadal VAT of aged male and female offspring of *Rank* ^{WT} (n = 7/6) and *Rank* $^{\Delta Foxn1}$ (n = 9/6) dams. Data are shown as box-and-whisker

Europe PMC Funders Author Manuscripts

plots (from minimal to maximal values) and each dot represents an individual mouse. *$P <$ 0.05. Two-tailed Student's *t*-test. **p**, Percentages of $CD4^+FOXP3^+T_{reg}$ cells (of total CD4) in the gonadal VAT of aged male and female offspring of $Rank^{WT}$ (n = 10/8) and $Rank^{\Delta Foxn1}$ (n = 12/9) dams. Data are shown as box-and-whisker plots (from minimal to maximal values) and each dot represents an individual mouse. **$P < 0.01$. Two-tailed Student's *t*-test. **q**, Percentages of $Cd11b^+F4/80^+$ macrophages (left) as well as percentage of M1 ($CD11c^+CD301^-$) and M2 ($CD11c^-CD301^+$) macrophages (right, gated on $Cd11b^+F4/80^+$ macrophages) in the gonadal white adipose tissue of aged male and female offspring of $Rank^{WT}$ and $Rank^{\Delta Foxn1}$ dams. Data are shown as box-and-whisker plots (from minimal to maximal values) and each dot represents an individual mouse, with n = 6–12 per group. **$P < 0.01$. Two-tailed Student's *t*-test. Data in **o**–**q** are from individual 15–17-month-old mice, fed a normal chow since weaning.

Europe PMC Funders Author Manuscripts

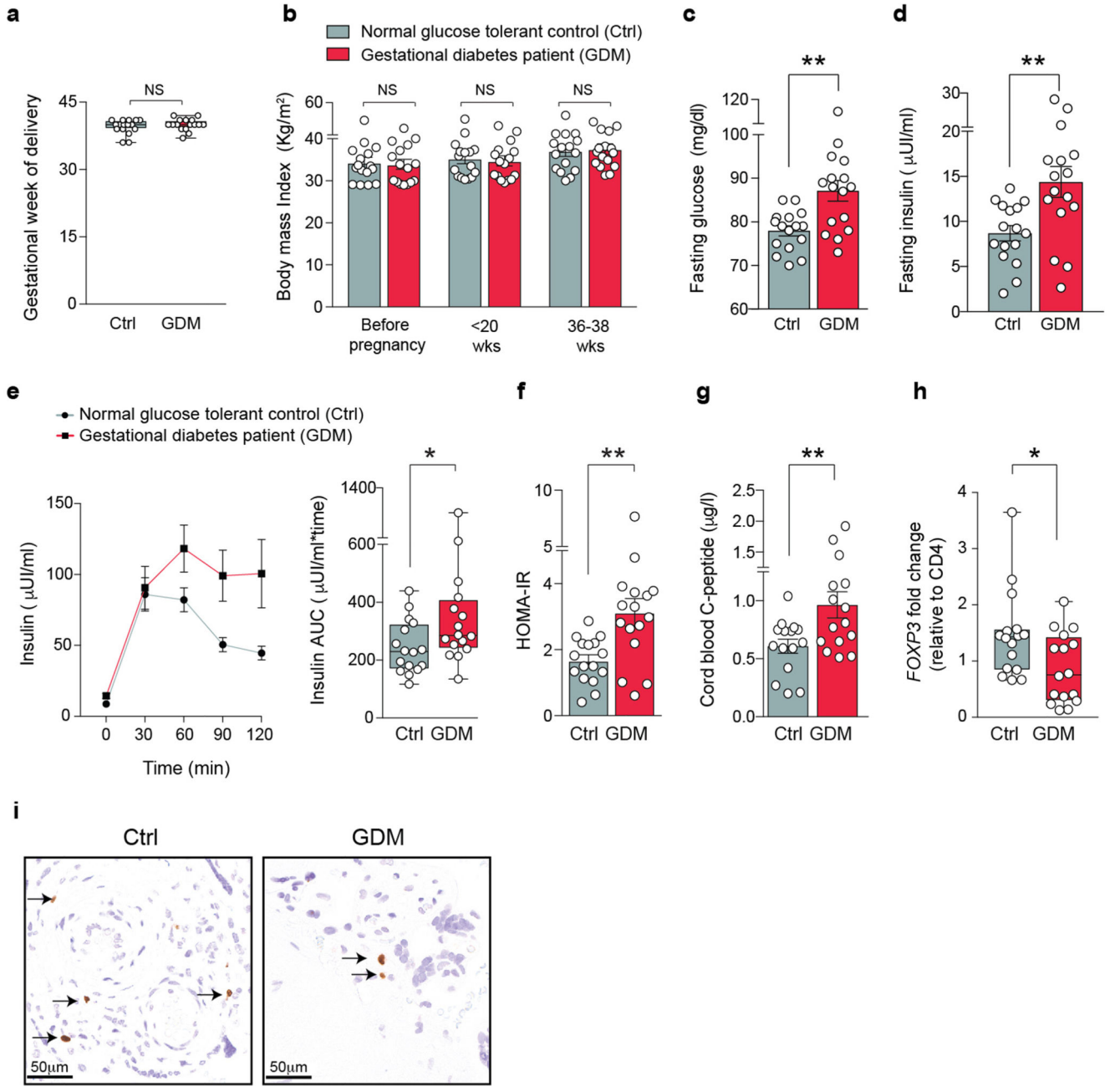

Extended Data Fig. 10. Characterization of human patients with GDM.

a, Gestational week of delivery for control glucose-tolerant pregnant women (Ctrl) and pregnant women with GDM included in the study. All women were carrying singleton pregnancies with equal distribution of sex in each group ($n = 8$ carrying female and $n = 8$ carrying male babies). Placenta samples were collected at delivery and were also matched for gestational week and sex of the baby. Data are shown as box-and-whisker plots (from minimal to maximal values) and each dot represents an individual woman, with $n = 16/16$ women per group. Two-tailed Mann–Whitney *U*-test. **b**, BMI before pregnancy, at early pregnancy (<20 weeks) and at late pregnancy (36–38 weeks) for control glucose-tolerant

Europe PMC Funders Author Manuscripts

pregnant women and pregnant women with GDM, showing matched BMI between the cohorts. Data are mean ± s.e.m. and each dot represents a woman $n = 16/16$. Two-tailed Student's *t*-test. **c**, **d**, Fasting glucose (**c**) and insulin (**d**) levels for pregnant women diagnosed with GDM as well as control glucose-tolerant pregnant women. $n = 16$ per group (data are mean ± s.e.m. and each dot represents an individual woman). $^{**}P < 0.01$. Two-tailed Student's *t*-test. **e**, Plasma insulin levels (mean ± s.e.m.) and the corresponding area under the curve calculations during the 2 h oral glucose test shown in Fig. 4g, for the same pregnant women with GDM and control pregnant women. Data are shown as box-and-whisker plots (from minimal to maximal values) and each dot represents an individual woman, with $n = 16$ per group. $^{*}P < 0.05$. two-tailed Mann–Whitney *U*-test. **f**, Homeostasis model assessment of insulin resistance (HOMA-IR) for the pregnant women with GDM as well as control glucose-tolerant pregnant women. Data are mean ± s.e.m. and each dot represents an individual woman, $n = 16/16$. $^{**}P < 0.01$. two-tailed Student's *t*-test. Data in **c**–**f** were collected at early gestation (<20 weeks). Similar results were observed mid- (24–28 weeks) and late pregnancy (36–38 weeks) (data not shown). **g**, Birth levels of C-peptide (a by-product of insulin production in the β-islets) in the cord blood of babies born to GDM ($n = 15$) and control glucose-tolerant mothers ($n = 15$), revealing hyperinsulinaemia in the babies of mothers with GDM. Data are mean ± s.e.m. and each dot represents an individual sample. $^{**}P < 0.01$. Two-tailed Student's *t*-test. **h**, Relative expression of the T_{reg}-cell-specific transcript *FOXP3* normalized to CD4 transcript levels in the placentas of control glucose-tolerant pregnant women ($n = 16$) and in pregnant women with GDM ($n = 16$). Three distal placental tissue slices (all on the maternal side) were analysed for each woman and then averaged. Note that similar results were observed if normalized to a housekeeping gene (shown in Fig. 4i, j). Data are shown as box-and-whisker plots (from minimal to maximal values) and each dot represents an individual woman. $^{*}P < 0.05$. Two-tailed Mann–Whitney *U*-test. **i**, Immunohistochemistry detecting $FOXP3^{+}T_{reg}$ cells (arrows) in the placentas of control glucose-tolerant pregnant controls and women with GDM. Representative of $n = 65/28$ slides analysed per group. For relative quantification of the staining see Fig. 4k.

Supplementary Material

Refer to Web version on PubMed Central for supplementary material.

Acknowledgements

We thank all members of the Penninger and Paolino laboratories for discussions and technical support; Y. Redouane for help with RNA isolation; D. Hoffmann and L. Haas for assistance with oral gavage and intravenous injections; S. Gavali for proofreading the manuscript; G. Schmauss, G. Petri, M. Weninger and other members of the IMP-IMBA Biooptics service facility for assistance in cell sorting and image quantification; staff of the VBCF histopathology department and, in particular, M. Zeba, J. Klughofer and A. Kavirayani, as well as H. Schachner for histology support; and staff of the animal facility and all other IMP/IMBA service facilities. Mass spectrometry and QuantSeq were performed at the VBCF Metabolomics and Next Generation Sequencing units, funded by the City of Vienna. Smart-seq2 libraries were sequenced by the Biomedical Sequencing Facility at CeMM. M.P. is a Ragnar Söderberg Fellow in Medicine and is supported by IMBA, start-up grants from the Karolinska Institutet, the Swedish Research Council (Vetenskapsrådet NE 2016-04458) and the Ragnar Söderberg Foundation (M21/17). G.A.H. is supported by grants from the Swiss National Foundation (3100-68310.02 and 3100-122558) and The Wellcome Trust (105045/Z/14/Z). J.P.F. is funded by Agencia Nacional de Promoción Científica y Tecnológica (PICT-2017-2401), GlaxoSimthKline/Ministerio de Ciencia y Técnica (PCE-GSK-2017-0052) and Fundación para el Progreso de la Medicina (GF-N03/2017). G.A. is supported by a MRC Programme Grant (MR/N000919/1),

A.J.W. is funded by a Wellcome Trust Seed Award (204375/Z/16/Z). L.K. is supported by the BM Fonds (15142), the Margaretha Hehberger Stiftung (15142), the COMET Competence Center CBmed (Center for Biomarker Research in Medicine) (FA791A0906.FFG), a FWF grant (P26011) and the Christian-Doppler Lab for Applied Metabolomics. A.K.-W. and J.H. are supported by the Austrian Science Fund No. I 4209 (GOING-FWD) and a Medical Scientific Fund of the Mayor of the City of Vienna (15205). J.M.P. is supported by the Austrian Federal Ministry of Education, Science and Research, the Austrian Academy of Sciences and the City of Vienna and grants from the Austrian Science Fund (FWF Wittgenstein award Z 271-B19), the T. von Zastrow foundation, an EU ERC Advanced Grant (European Community's Seventh Framework Programme (FP7/2007-2013)/ERC grant agreement no. 341036) and a Canada 150 Research Chairs Program (F18-01336).

Data availability

RNA-sequencing data has been deposited in the NCBI Gene Expression Omnibus under the following accession numbers: QuantSeq data on VAT tissue: GSE117112; Smart-seq2 data on T_{reg} cells: GSE97666.

References

1. Soma-Pillay P, Nelson-Piercy C, Tolppanen H, Mebazaa A. Physiological changes in pregnancy. Cardiovasc J Afr. 2016; 27:89–94. [PubMed: 27213856]
2. Arck PC, Hecher K. Fetomaternal immune cross-talk and its consequences for maternal and offspring's health. Nat Med. 2013; 19:548–556. [PubMed: 23652115]
3. Persike EC Jr. Involution of the thymus during pregnancy in young mice. Proc Soc Exp Biol Med. 1940; 45:315–317.
4. Dougall WC, et al. RANK is essential for osteoclast and lymph node development. Genes Dev. 1999; 13:2412–2424. [PubMed: 10500098]
5. Kong Y-Y, et al. OPGL is a key regulator of osteoclastogenesis, lymphocyte development and lymph-node organogenesis. Nature. 1999; 397:315–323. [PubMed: 9950424]
6. Sigl V, Jones LP, Penninger JM. RANKL/RANK: from bone loss to the prevention of breast cancer. Open Biol. 2016; 6
7. Fata JE, et al. The osteoclast differentiation factor osteoprotegerin-ligand is essential for mammary gland development. Cell. 2000; 103:41–50. [PubMed: 11051546]
8. Rossi SW, et al. RANK signals from $CD4^{+}3^{-}$ inducer cells regulate development of Aire-expressing epithelial cells in the thymic medulla. J Exp Med. 2007; 204:1267–1272. [PubMed: 17502664]
9. Cowan JE, et al. The thymic medulla is required for $Foxp3^{+}$ regulatory but not conventional $CD4^{+}$Thymocyte development. J Exp Med. 2013; 210:675–681. [PubMed: 23530124]
10. Yadav M, et al. Neuropilin-1 distinguishes natural and inducible regulatory T cells among regulatory T cell subsets in vivo. J Exp Med. 2012; 209:1713–1722. [PubMed: 22966003]
11. Tilburgs T, et al. Evidence for a selective migration of fetus-specific $CD4^{+}CD25^{bright}$ regulatory T cells from the peripheral blood to the decidua in human pregnancy. J Immunol. 2008; 180:5737–5745. [PubMed: 18390759]
12. Aluvihare VR, Kallikourdis M, Betz AG. Regulatory T cells mediate maternal tolerance to the fetus. Nat Immunol. 2004; 5:266–271. [PubMed: 14758358]
13. Thornton AM, et al. Expression of Helios, an Ikaros transcription factor family member, differentiates thymic-derived from peripherally induced $Foxp3^{+}$T regulatory cells. J Immunol. 2010; 184:3433–3441. [PubMed: 20181882]
14. Kc K, Shakya S, Zhang H. Gestational diabetes mellitus and macrosomia: a literature review. Ann Nutr Metab. 2015; 66:14–20.
15. Kühl C. Glucose metabolism during and after pregnancy in normal and gestational diabetic women. 1. Influence of normal pregnancy on serum glucose and insulin concentration during basal fasting conditions and after a challenge with glucose. Acta Endocrinol (Copenh.). 1975; 79:709–719. [PubMed: 1173969]
16. Van Assche FA, Aerts L, De Prins F. A morphological study of the endocrine pancreas in human pregnancy. Br J Obstet Gynaecol. 1978; 85:818–820. [PubMed: 363135]

17. Kolodin D, et al. Antigen- and cytokine-driven accumulation of regulatory T cells in visceral adipose tissue of lean mice. Cell Metab. 2015; 21:543–557. [PubMed: 25863247]
18. Feuerer M, et al. Lean, but not obese, fat is enriched for a unique population of regulatory T cells that affect metabolic parameters. Nat Med. 2009; 15:930–939. [PubMed: 19633656]
19. Bapat SP, et al. Depletion of fat-resident T_{reg} cells prevents age-associated insulin resistance. Nature. 2015; 528:137–141. [PubMed: 26580014]
20. Hotamisligil GS, Shargill NS, Spiegelman BM. Adipose expression of tumor necrosis factor-alpha: direct role in obesity-linked insulin resistance. Science. 1993; 259:87–91. [PubMed: 7678183]
21. Vernochet C, et al. Adipose-specific deletion of TFAM increases mitochondrial oxidation and protects mice against obesity and insulin resistance. Cell Metab. 2012; 16:765–776. [PubMed: 23168219]
22. Boney CM, Verma A, Tucker R, Vohr BR. Metabolic syndrome in childhood: association with birth weight, maternal obesity, and gestational diabetes mellitus. Pediatrics. 2005; 115:e290–e296. [PubMed: 15741354]
23. Vohr BR, McGarvey ST, Tucker R. Effects of maternal gestational diabetes on offspring adiposity at 4–7 years of age. Diabetes Care. 1999; 22:1284–1291. [PubMed: 10480772]
24. Meier JJ, Bhushan A, Butler AE, Rizza RA, Butler PC. Sustained beta cell apoptosis in patients with long-standing type 1 diabetes: indirect evidence for islet regeneration? Diabetologia. 2005; 48:2221–2228. [PubMed: 16205882]
25. Butler AE, et al. β-Cell deficit and increased β-cell apoptosis in humans with type 2 diabetes. Diabetes. 2003; 52:102–110. [PubMed: 12502499]
26. Sacks DA, et al. Frequency of gestational diabetes mellitus at collaborating centers based on IADPSG consensus panel-recommended criteria: the Hyperglycemia and Adverse Pregnancy Outcome (HAPO) study. Diabetes Care. 2012; 35:526–528. [PubMed: 22355019]
27. Egan AM, et al. Epidemiology of gestational diabetes mellitus according to IADPSG/WHO 2013 criteria among obese pregnant women in Europe. Diabetologia. 2017; 60:1913–1921. [PubMed: 28702810]
28. Somerset DA, Zheng Y, Kilby MD, Sansom DM, Drayson MT. Normal human pregnancy is associated with an elevation in the immune suppressive $CD25^+$ $CD4^+$ regulatory T-cell subset. Immunology. 2004; 112:38–43. [PubMed: 15096182]
29. Zenclussen AC, et al. Abnormal T-cell reactivity against paternal antigens in spontaneous abortion: adoptive transfer of pregnancy-induced $CD4^+CD25^+$T regulatory cells prevents fetal rejection in a murine abortion model. Am J Pathol. 2005; 166:811–822. [PubMed: 15743793]
30. Sansom SN, et al. Population and single-cell genomics reveal the Aire dependency, relief from Polycomb silencing, and distribution of self-antigen expression in thymic epithelia. Genome Res. 2014; 24:1918–1931. [PubMed: 25224068]
31. St-Pierre C, Trofimov A, Brochu S, Lemieux S, Perreault C. Differential features of AIRE-induced and AIRE-independent promiscuous gene expression in thymic epithelial cells. J Immunol. 2015; 195:498–506. [PubMed: 26034170]
32. Butte NF. Carbohydrate and lipid metabolism in pregnancy: normal compared with gestational diabetes mellitus. Am J Clin Nutr. 2000; 71:1256S–1261S. [PubMed: 10799399]
33. Bellamy L, Casas J-P, Hingorani AD, Williams D. Type 2 diabetes mellitus after gestational diabetes: a systematic review and meta-analysis. Lancet. 2009; 373:1773–1779. [PubMed: 19465232]
34. Clausen TD, et al. High prevalence of type 2 diabetes and pre-diabetes in adult offspring of women with gestational diabetes mellitus or type 1 diabetes: the role of intrauterine hyperglycemia. Diabetes Care. 2008; 31:340–346. [PubMed: 18000174]
35. Hanada R, et al. Central control of fever and female body temperature by RANKL/RANK. Nature. 2009; 462:505–509. [PubMed: 19940926]
36. Zuklys S, et al. Stabilized β-catenin in thymic epithelial cells blocks thymus development and function. J Immunol. 2009; 182:2997–3007. [PubMed: 19234195]
37. Fontenot JD, et al. Regulatory T cell lineage specification by the Forkhead transcription factor Foxp3. Immunity. 2005; 22:329–341. [PubMed: 15780990]

38. Tarutani M, et al. Tissue-specific knockout of the mouse *Pig-a* gene reveals important roles for GPI-anchored proteins in skin development. Proc Natl Acad Sci USA. 1997; 94:7400–7405. [PubMed: 9207103]
39. Weiss JM, et al. Neuropilin 1 is expressed on thymus-derived natural regulatory T cells, but not mucosa-generated induced Foxp3^{+}T reg cells. J Exp Med. 2012; 209:1723–1742. [PubMed: 22966001]
40. Idris AI. Ovariectomy/orchidectomy in rodents. Methods Mol Biol. 2012; 816:545–551. [PubMed: 22130951]
41. Xing Y, Hogquist KA. Isolation, identification, and purification of murine thymic epithelial cells. J Vis Exp. 2014; 90:e51780.
42. Picelli S, et al. Full-length RNA-seq from single cells using Smart-seq2. Nat Protocols. 2014; 9:171–181. [PubMed: 24385147]
43. Dobin A, et al. STAR: ultrafast universal RNA-seq aligner. Bioinformatics. 2013; 29:15–21. [PubMed: 23104886]
44. Love MI, Huber W, Anders S. Moderated estimation of fold change and dispersion for RNA-seq data with DESeq2. Genome Biol. 2014; 15:550. [PubMed: 25516281]
45. Wickham, H. ggplot2: Elegant Graphics for Data Analysis. Springer; 2016.
46. Bolotin DA, et al. MiXCR: software for comprehensive adaptive immunity profiling. Nat Methods. 2015; 12:380–381. [PubMed: 25924071]
47. Anderson MS, et al. Projection of an immunological self shadow within the thymus by the Aire protein. Science. 2002; 298:1395–1401. [PubMed: 12376594]
48. Harreiter J, et al. IADPSG and WHO 2013 gestational diabetes mellitus criteria identify obese women with marked insulin resistance in early pregnancy. Diabetes Care. 2016; 39:e90–e92. [PubMed: 27208336]
49. Metzger BE, et al. International association of diabetes and pregnancy study groups recommendations on the diagnosis and classification of hyperglycemia in pregnancy. Diabetes Care. 2010; 33:e98.
50. Diagnostic criteria and classification of hyperglycaemia first detected in pregnancy: a World Health Organization Guideline. Diabetes Res Clin Pract. 2014; 103:341–363. [PubMed: 24847517]

Europe PMC Funders Author Manuscripts

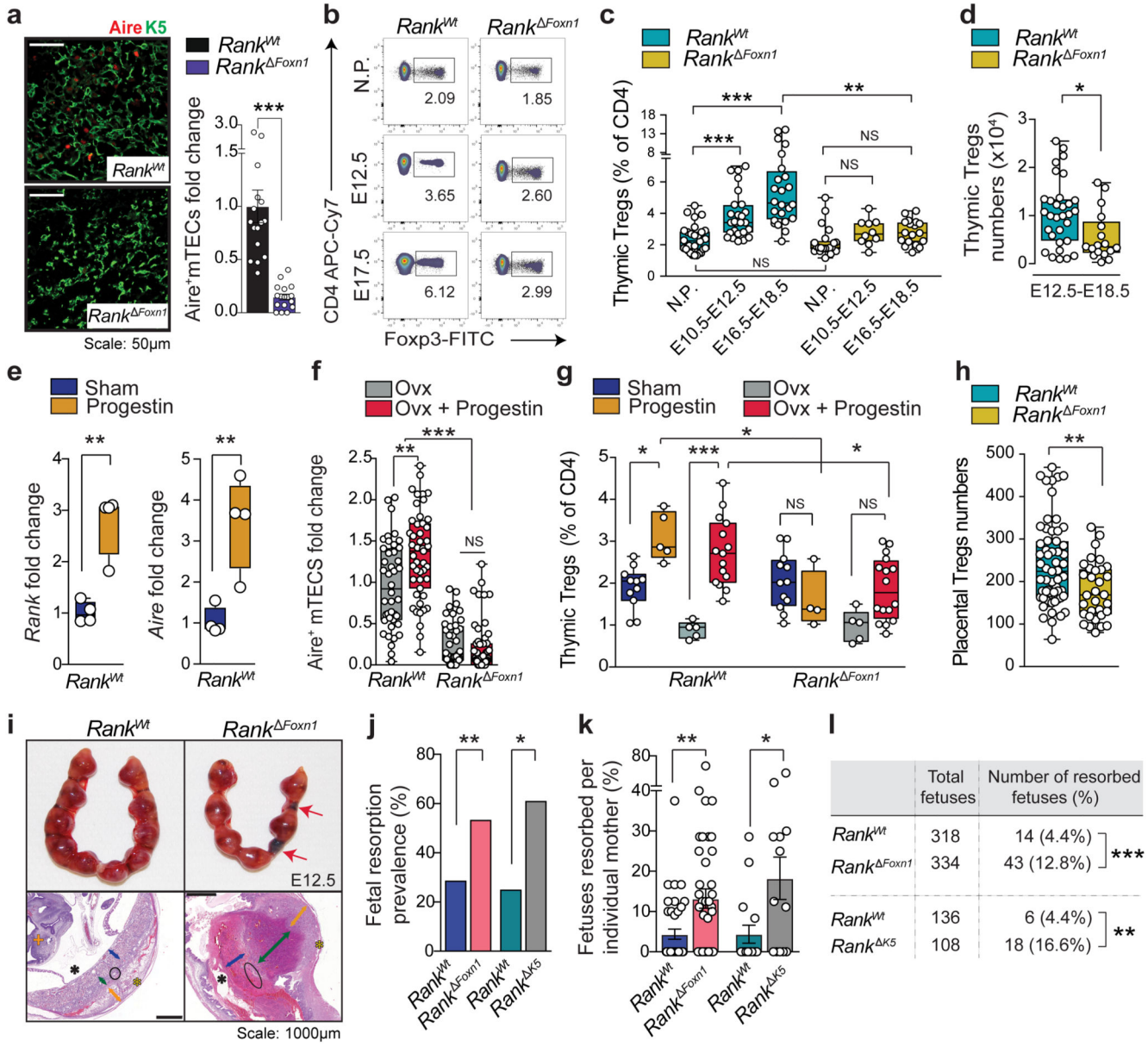

Fig. 1. RANK-expressing mTECs control thymic T_{reg} cell expansion in pregnancy.

a, AIRE and K5 staining in thymic cross-sections and relative numbers of AIRE$^+$mTECs in *Rank* ^{WT} and *Rank* $^{\Delta Foxn1}$ mice (n = 4, 4–6 fields per mouse). Scale bar, 50 μm. **b**, Fluorescence-activated cell sorting (FACS) plots for CD4$^+$FOXP3$^+$$T_{reg}$ cells in the thymus of non-pregnant (NP), and pregnant *Rank* ^{WT} and *Rank* $^{\Delta Foxn1}$ mice at E12.5 and E17.5 (the gating strategy is shown in Supplementary Data 1). **c**, Percentages of CD4$^+$FOXP3$^+$$T_{reg}$ cells in the thymus of non-pregnant, mid-pregnant (E10.5–E12.5) and late pregnant (E16.5–E18.5) *Rank* ^{WT} and *Rank* $^{\Delta Foxn1}$ females (n = 10–28). **d**, Numbers of CD4$^+$FOXP3$^+$$T_{reg}$ cells in the thymus of *Rank* ^{WT} and *Rank* $^{\Delta Foxn1}$ pregnant mice at E12.5–E18.5 (n = 31/17 for *Rank* ^{WT}/*Rank* $^{\Delta Foxn1}$ mice, respectively. **e**, *Rank* and *Aire* mRNA expression in the thymic stroma of sham- or progestin-treated *Rank* ^{WT} female mice (n = 4). **f**, AIRE$^+$mTECs

in ovariectomized (Ovx, n = 7/8), and ovariectomized and progestin-treated (n = 8/11) *Rank* ^{WT} and *Rank* $^{\Delta Foxn1}$ female mice (5–6 fields per mouse). **g**, Percentages of $CD4^+FOXP3^+$ Thymic T_{reg} cells in sham-treated (n = 11/12), progestin-treated (n = 5/4), ovariectomized (n = 5/5), and ovariectomized and progestin-treated (n = 15/16) *Rank* ^{WT} and *Rank* $^{\Delta Foxn1}$ female mice. **h**, Numbers of $CD4^+FOXP3^+T_{reg}$ cells in E17.5 placentas of *Rank* ^{WT} and *Rank* $^{\Delta Foxn1}$ mice. n = 59/32 placentas from n = 11/8 dams. **i**, Top, uterine horns of *Rank* ^{WT} and *Rank* $^{\Delta Foxn1}$ dams displaying placental–fetus units. Images are representative of n = 10/9. Red arrows show fetal resorption. Bottom, congested and widened spongiotrophoblast (green arrows), necrotic labyrinth (blue arrows) and trophoblast giant cells (black circles) in placental cross-sections stained with haematoxylin and eosin (images are representative of n = 29/30 placentas). Orange arrows, decidua basalis; yellow asterisks, mesometrial lymphoid aggregate of pregnancy; black asterisks, amnion cavity; orange cross, embryo. Scale bars, 1,000 μm. **j**, **k**, Prevalence (percentage of mice with at least one fetal resorption) (**j**) and percentages (**k**) of fetal resorption in *Rank* ^{WT} and *Rank* $^{\Delta Foxn1}$ (n = 40/40), and *Rank* ^{WT} and *Rank* $^{\Delta K5}$ (n = 16/13) dams at E12.5–E18.5. **l**, Numbers and percentages of resorbed fetuses in *Rank* ^{WT} and *Rank* $^{\Delta Foxn1}$ (n = 41/42), and *Rank* ^{WT} and *Rank* $^{\Delta K5}$ (n = 16/13) dams at E12.5–E18.5. Data are shown as bar graphs (**a**, **k**; mean ± s.e.m.), and box-and-whisker plots (**c**–**h**, from minimal to maximal values. Dots represent individual data points. $^*P < 0.05$; $^{**}P < 0.01$; $^{***}P < 0.001$; NS, not significant. Two-tailed Student's t-test (**a**, **e**); Kruskal–Wallis test with Dunn's post-test (**c**); two-tailed Mann–Whitney U-test (**d**, **h**, **k**); one-way analysis of variance (ANOVA) with Tukey's post hoc test (**f**, **g**); two-tailed χ^2 test (**j**, **l**).

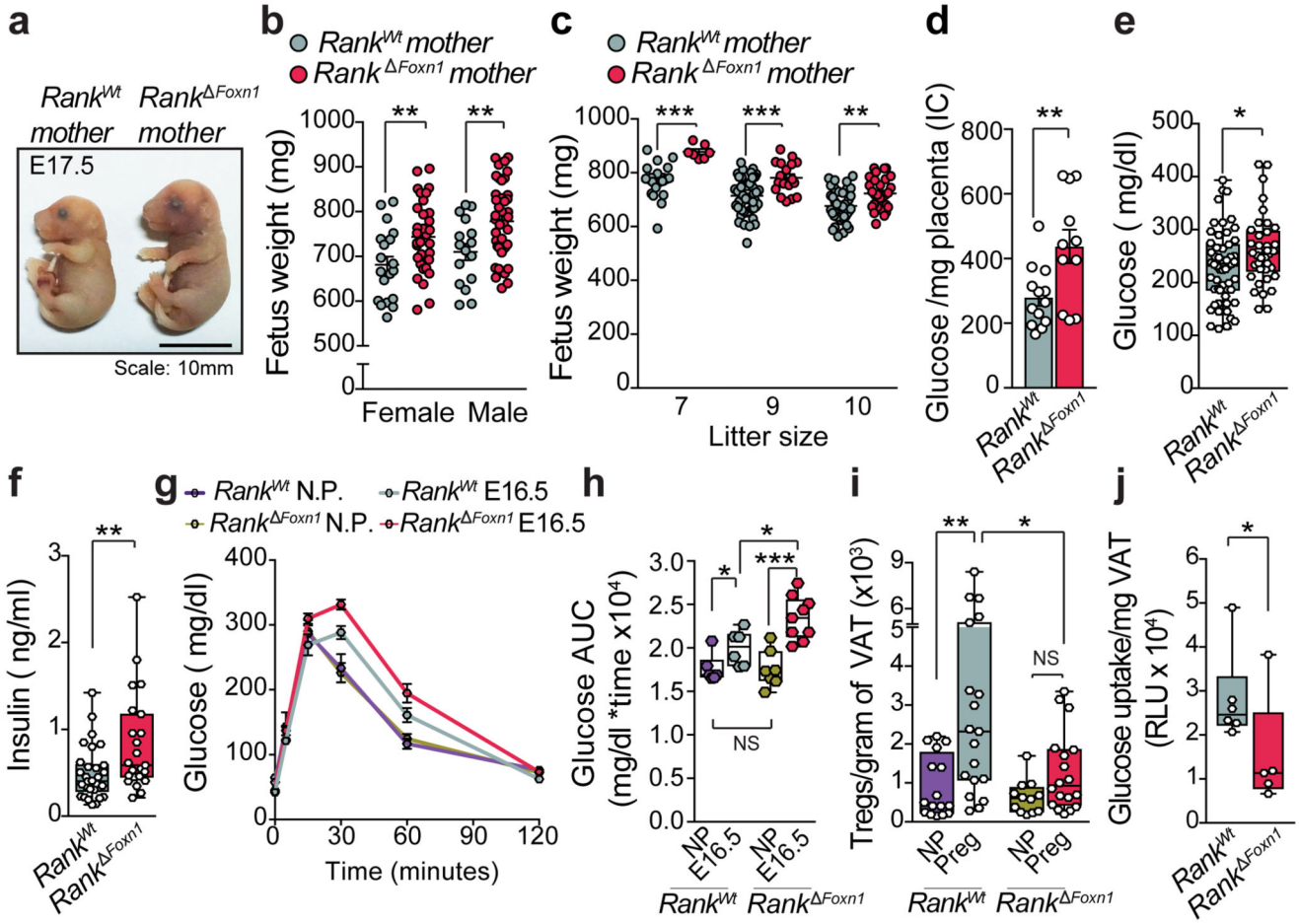

Fig. 2. Loss of *Rank* in mTECs augments gestational glucose intolerance.

a, Sizes of fetuses from *Rank* ^{WT} or *Rank* $^{\Delta Foxn1}$ mothers at E17.5. Scale bar, 10 mm. **b**, **c**, Macrosomia of E17.5 fetuses gestated in *Rank* $^{\Delta Foxn1}$ dams independent of sex (**b**) or litter size (**c**). n = 7–42 fetuses. **d**, Glucose levels in placentas of *Rank* ^{WT} and *Rank* $^{\Delta Foxn1}$ dams at E17.5 (n = 13/11 placentas from 4/5 dams). IC, ion current. **e**, **f**, Ad libitum-fed serum levels of glucose (**e**, n = 55/38) and insulin (**f**, n = 30/23) in pregnant (E12.5–E18.5) *Rank* ^{WT} and *Rank* $^{\Delta Foxn1}$ female mice. **g**, **h**, Oral glucose-tolerance test (mean ± s.e.m.) (**g**) and the corresponding area under the curve (AUC) (**h**) of non-pregnant (n = 6/7) and pregnant (E16.5) (n = 6/9) *Rank* ^{WT} and *Rank* $^{\Delta Foxn1}$ female mice. **i**, Total numbers of $CD4^+FOXP3^+T_{reg}$ cells in gonadal VAT of non-pregnant (n = 16/12) and pregnant (Preg, n = 19/18, E13.5–E17.5 pool) *Rank* ^{WT} and *Rank* $^{\Delta Foxn1}$ females. **j**, Uptake of 2-deoxyglucose in visceral adipose tissue of *Rank* ^{WT} and *Rank* $^{\Delta Foxn1}$ dams at E17.5. n = 6/5. RLU = relative luminescent units. Data are shown as bar charts, scatter dot plots (**b-d**, mean ± s.e.m.) and box-and-whisker plots (**e,f,h-j**, from minimal to maximal values). Dots represent individual data points. *P < 0.05; **P < 0.01; ***P < 0.001. Two-tailed Student's t-test for **b-e**; two-tailed Mann–Whitney U-test for **f,h,j**; One-way ANOVA, Tukey's post hoc for **i**.

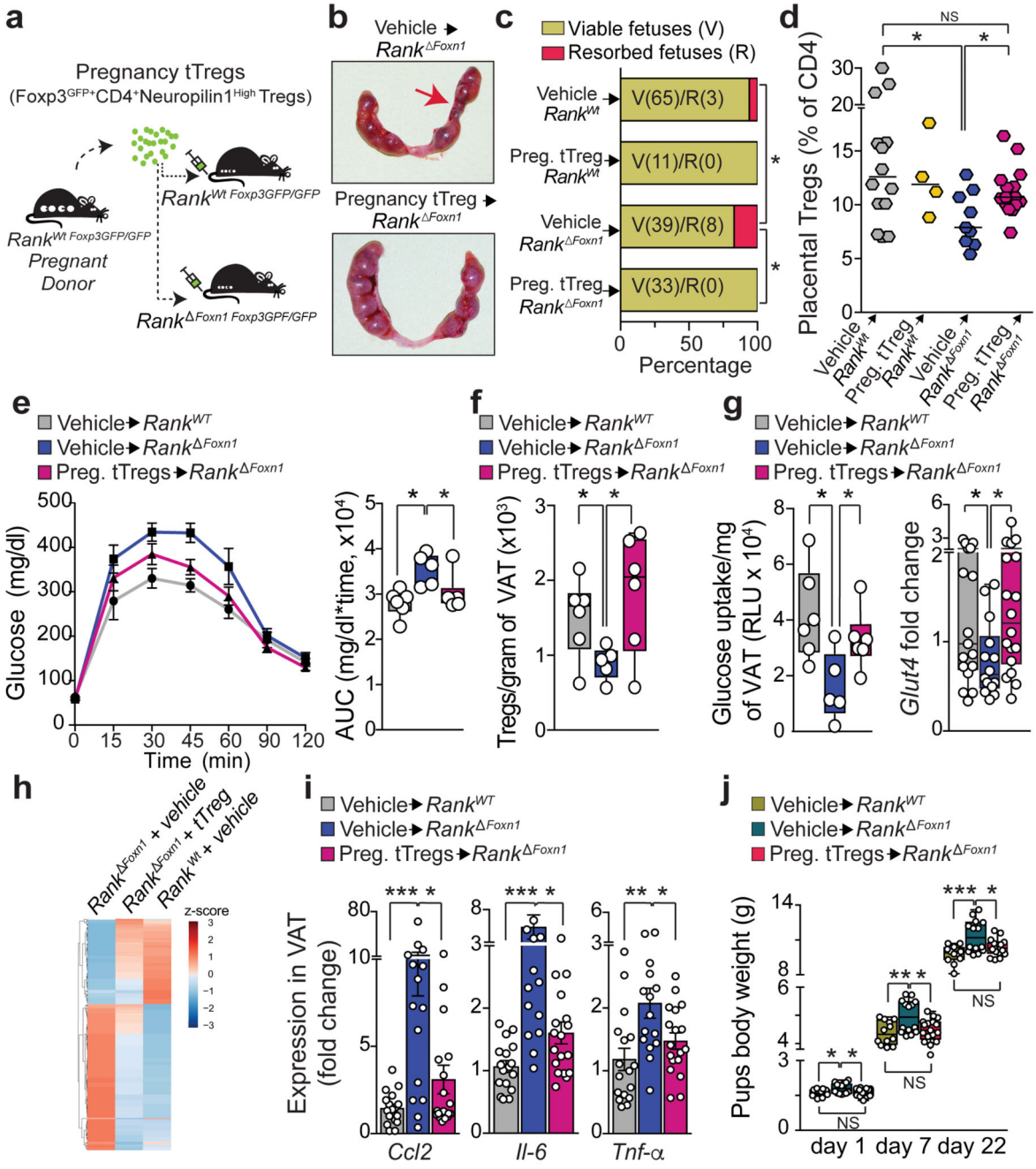

Fig. 3. T_{reg} cells rescue fetal tolerance and maternal glucose metabolism.

a, Schematic of T_{reg} cell adoptive transfer of pregnancy thymic T_{reg} cells (Foxp3–GFP $^{+}CD4^{+}$neuropilin-1^{high} T_{reg} cells). For details, see Methods. **b**, Uterine horns of *Rank* $^{\Delta Foxn1}$ dams treated with vehicle (PBS) or pregnancy thymic T_{reg} cells. Arrow shows fetal resorption. **c**, Percentages and total numbers of viable and resorpted fetuses gestated in *Rank* ^{WT} and *Rank* $^{\Delta Foxn1}$ pregnant mice, treated with vehicle or pregnancy thymic T_{reg} cells. n = 8/2/6/4 dams. **d**, Percentage of $CD4^{+}FOXP3^{+}T_{reg}$ cells in E12.5 placentas of *Rank* ^{WT} and *Rank* $^{\Delta Foxn1}$ dams receiving vehicle or pregnancy thymic T_{reg} cells. n = 14/4/9/15. **e**–**g**, Oral

Europe PMC Funders Author Manuscripts

glucose-tolerance test (mean ± s.e.m.) and corresponding area under the curve (**e**), numbers of $CD4^+FOXP3^+T_{reg}$ cells in gonadal VAT (**f**) and insulin-stimulated 2-deoxyglucose uptake and relative expression of the glucose transporter *Glut4* (**g**) in the VAT of vehicle-treated $Rank^{WT}$ ($n = 6$) and vehicle- and pregnancy thymic T_{reg} cell-treated $Rank^{\Delta Foxn1}$ ($n = 5/6$) dams at E16.5 (**e**, **f**) and E17.5 (**g**, 2 VAT samples per mouse). RLU, relative luminescent units. **h**, Relative expression levels of differentially expressed genes in the pairwise comparisons (DESeq2 v.1.16.1, false-discovery rate (FDR) threshold of 0.05). $n = 4$. **i**, *Ccl2*, *Il6* and *Tnf* qPCR expression in VAT of vehicle-treated $Rank^{WT}$ ($n = 6$) and vehicle- and pregnancy thymic T_{reg} cell-treated $Rank^{\Delta Foxn1}$ ($n = 5/6$) dams at E17.5 (3 VAT samples per mouse). **j**, Body weights of pups, born to the indicated mothers, at perinatal and weaning ages ($n = 12/14/17$). Data are shown as scatter dot plots (**d**, lines are median), bar charts (**i**, mean ± s.e.m.) and box-and-whisker plots (**e**–**g**, **j**, from minimal to maximal values. Dots represent individual data points. $^*P < 0.05$; $^{**}P < 0.01$; $^{***}P < 0.001$. Two-tailed χ^2 test (**c**); Student's *t*-test (**d**, **f**, **g**); two-tailed Mann–Whitney *U*-test (**i**); Kruskal–Wallis test with Dunn's post-test (**e**); one-way ANOVA with Tukey's post hoc test (**j**).

Europe PMC Funders Author Manuscripts

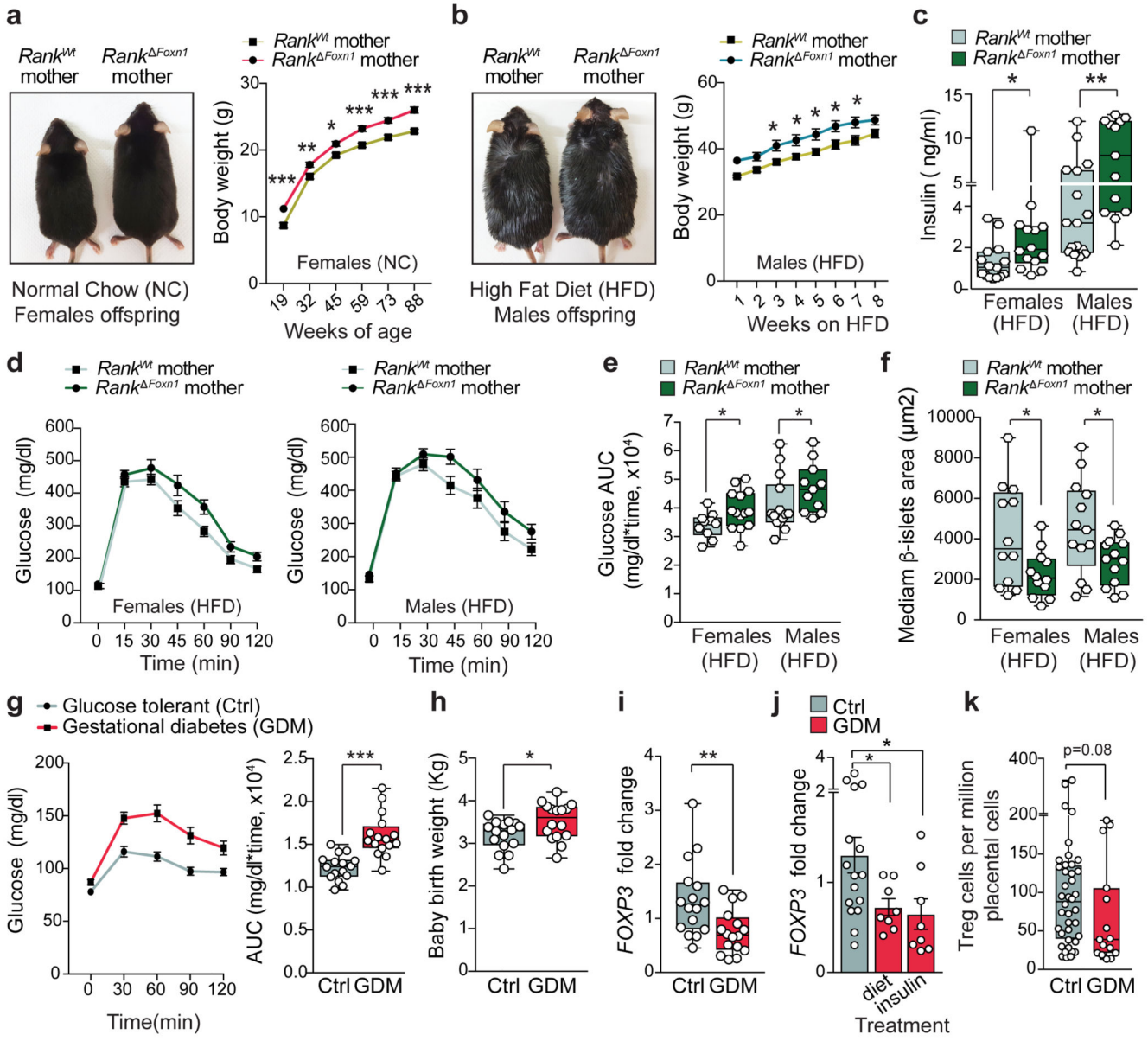

Fig. 4. Transgenerational metabolic disorders in the offspring of *Rank* $^{\Delta Foxn1}$ mothers.

a, Body weights (mean ± s.e.m.) of the female offspring of *Rank* ^{WT} and *Rank* $^{\Delta Foxn1}$ dams (n = 15 and 14) fed normal chow. Image, 80-day-old mice. **b**, Photograph (6 weeks on HFD) and body weights (mean ± s.e.m.) of male offspring of *Rank* ^{WT} and *Rank* $^{\Delta Foxn1}$ dams (n = 16/11) fed an HFD. **c**–**e**, Ad libitum-fed serum insulin levels in female (n = 15/14) and male (n = 17/13) offspring of *Rank* ^{WT} and *Rank* $^{\Delta Foxn1}$dams (**c**), oral glucose-tolerance test (mean ± s.e.m.) (**d**) and area under the curve (**e**) for female (n = 14/10) and male (n = 14/11) offspring of *Rank* ^{WT} and *Rank* $^{\Delta Foxn1}$ dams fed a HFD for 9 weeks. **f**, Median β-islets area in female (n = 12/12) and male (n = 13/13) offspring of *Rank* ^{WT} and *Rank* $^{\Delta Foxn1}$ dams on HFD for 12 weeks. **g**, Oral glucose-tolerance test (mean ± s.e.m.) and area under the curve for pregnant women with gestational diabetes mellitus (GDM) and a glucose-tolerant

pregnant control group (control). $n = 16/16$. **h**, Birth weights of babies born to mothers with gestational diabetes and control mothers ($n = 16/16$). **i**, *FOXP3* transcripts in the placentas of control pregnant women and pregnant women with gestational diabetes ($n = 16/16$). **j**, *FOXP3* transcripts in the placentas of control pregnant women and pregnant women with gestational diabetes treated with a controlled diet or by administration of insulin (mean ± s.e.m., $n = 16/8/8$). **k**, $FOXP3^{+}T_{reg}$ cells in the placentas (maternal side) of control pregnant women and pregnant women with gestational diabetes ($n = 17/8$) detected by immunohistochemistry (2–3 sites per placenta). Data in **c**, **e**–**i**, **k** are shown as box-and-whisker plots (from minimal to maximal values). Dots represent individual data points. $*P < 0.05$; $**P < 0.01$; $***P < 0.001$. Two-way ANOVA with Sidak's multiple comparison (**a**, **b**); two-tailed Mann–Whitney *U*-test (**c**, **e**, **g**, **i**–**k**); two-tailed Student's *t*-test (**f**, **h**).

Europe PMC Funders Author Manuscripts